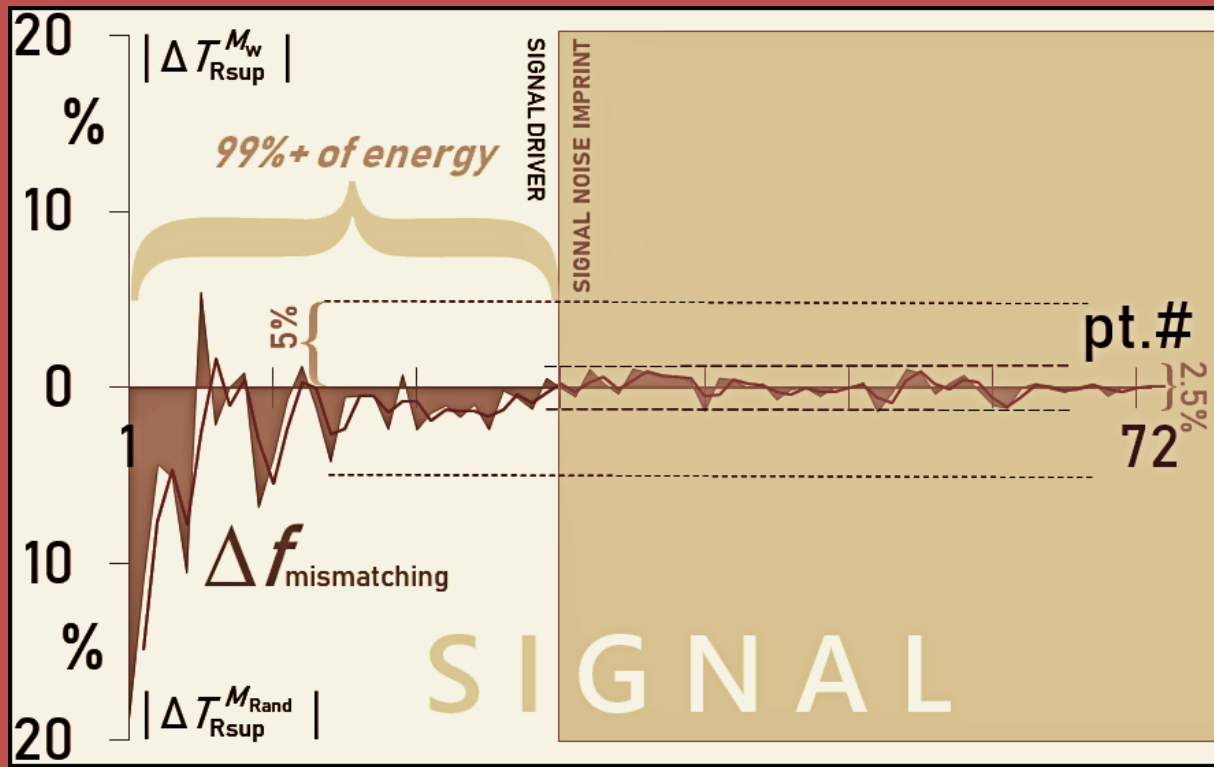
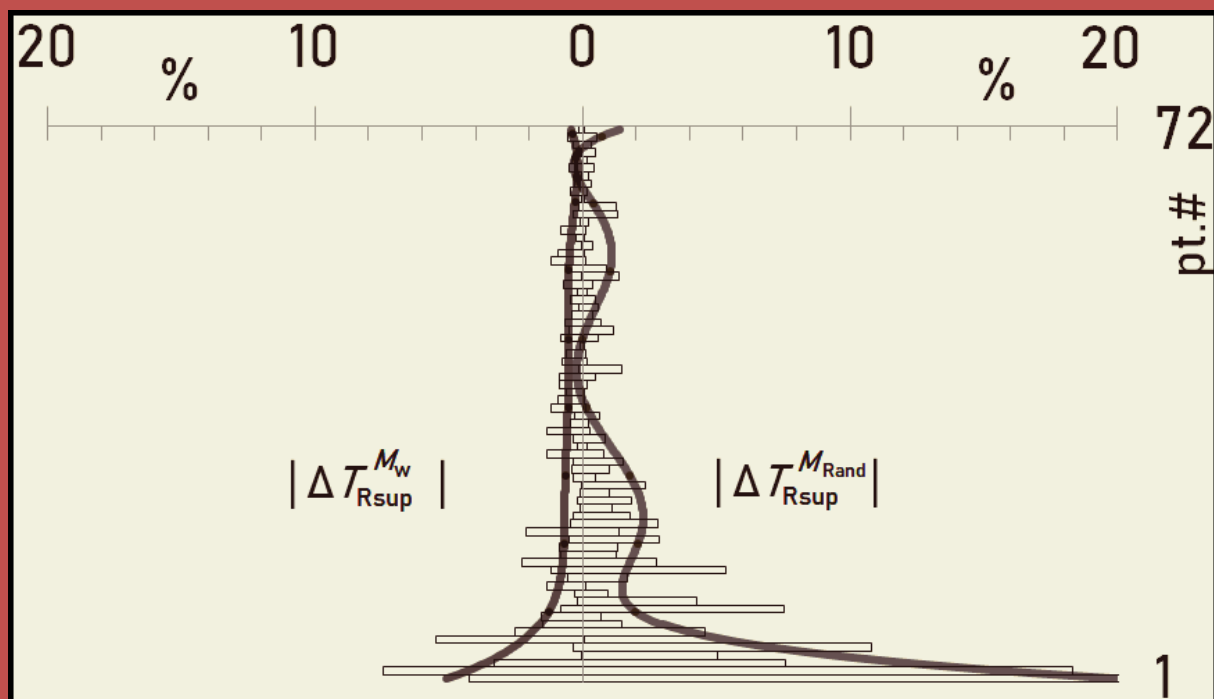


Cover art



Real-data spectra seen outperforming random-data spectra in matching the 72h period-forced superharmonic resonance's 72 theoretical subperiods, by 350% (as measured by the ratio of respective weighted averages of the matches). The mismatching (differencing) discrete function Δf strongly favors the random-data spectra.



Absolute outperformance of real-data (M_w seismic magnitudes) spectra over random-data spectra in matching the 72h period-forced superharmonic resonance's 72 theoretical subperiods. Polynomial trendlines overlaid.

Earth Body Resonance

Mensur Omerbashich

PO Box 1, Sarajevo Bosnia | hm@royalfamily.ba

The full range of 72h-forced, 72 superharmonic resonance periods, is detected in time-series of all 866 earthquakes of robust $M_w 5.6+$ from USGS, EMSC, and GFZ, 2015-19 catalogs. The resonance is in the 55'–15 days long-periodic band (0.303 mHz–0.771605 μ Hz) at 99–67% confidence. Moreover, omitting of the 21 overrepresenting events has improved the result. The signal is clear, strong, and stable – demonstrating beyond doubt that $M_w 6.2+$ seismicity arises due to long-periodic resonance. Remarkably, the natural mode's cluster was detected too; it averaged 60.1', while the absolutely strongest resonance period was also 59.9', at 2.3 var%, or to within the 1Hz sampling rate – revealing that the 72 h forcer is the modulator of the Earth's natural period via synchronization. The dominance property of the forcer also follows from detection of its many other fractional multiples: $^{14}/_5, ^3/_2, ^5/_12, ^5/_36$, etc. After Schumann resonance discovery in the short band (extremely long band of the EM Spectrum), this is the second report ever of a full resonance bundle in any global data and the first ever in tectonic earthquakes occurrences. The $M_w 6.2+$ seismotectonics arises via resonance-rupture response of tectonic plates and regions to the resonant phase or its fractional multiples. Fundamental questions of geophysics including earthquake prediction can be solved if the Earth is taken to be a many-oscillator nonlinear system. As an immediate benefit, the find enables a reliable partial seismic anti-forecasting (prediction of seismic quiescence), months ahead globally. This discovery of mechanically induced extreme-band energy on Earth invalidates the main (heat-transfer) geophysical hypothesis and thus should drastically diminish the role of chemistry in geosciences, specifically of geochemistry.

resonance; seismogenesis; tectonogenesis; tectonics; earthquakes; earthquake prediction; seismic forecasting

1. Introduction

Earlier, I postulated the *georesonator hypothesis* – thus challenging the currently favored heat-transfer hypothesis. Under the georesonator hypothesis, the Earth is a mechanical oscillator whose oscillations get magnified due to the stirring of masses induced by rotating Earth's one or two simultaneous conjunctions within our Solar system's plane and lasting for 3 or more days dynamically. Subsequently, oscillator equations, which describe forced vibrations with nonlinear damping, were applied for usual Earth parameters including viscosity to the Earth-Moon gravitational system as our planet's initiating interface with the band of extreme astrophysical energies. The well-known maximum displacement on Earth, of ~ 10 m, as well as the said conjunctive phase (natural period of Earth's mechanical resonances under external forcing by the Moon as the largest forcer), of $\varphi = 3$ days, are solutions of those equations. (Omerbashich, 2007)

To give a proof-in-principle of the correctness of the above approach, I then derived an absolute mathematical generalization of such a local setup by extending it from our Solar system on to the infinite number of universes. The generalization, which constitutes the basis of the corresponding *hyperresonance theory*, has resulted in the only known analytical expression for the Newtonian proportionality G (and thus for the Newtonian gravity too) via speed of light, while relating the Earth's mass oscillations with our Moon's orbital period at both macroscopic and quantum scales (Omerbashich, 2006a). Basically, by expanding on Tesla's work in mechanical-vibration-induced geophysics (Tesla, 1919), I was able to corroborate a relationship between gravity and speed of light, as proposed for our Solar system by Einstein in his rare work in geophysics (Schröder & Treder, 1997).

Because I regard the total-mass Earth as related to the entire Solar system and since varying distributions forbid reliable statistical tests and analyses, I subsequently gave a methodological proof – a pattern in the $M_w 5.6+$ earthquake occurrences (Omerbashich, 2016). The pattern depicts a real phenomenon, as seen from the fact that the pattern resolves better with the lithosphere's response to $M_w 6.2+$ earthquake sequences of three or more, Figure 1.

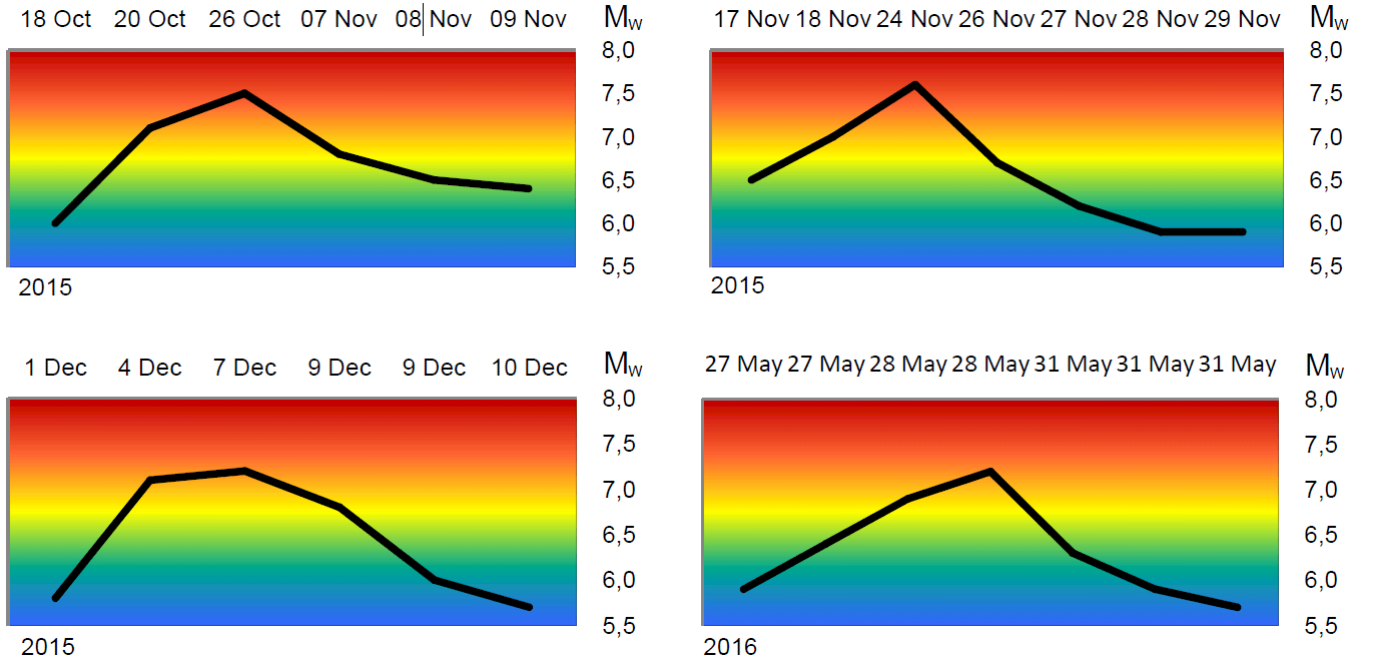


Figure 1. A pattern as found in $M_w 5.6+$ seismicity during Earth's conjunctions to heavenly bodies in our Solar system's plane that last for the duration of Earth's 3-day phase or longer. The physics behind the pattern is real because of resolution increase with the Earth's response to three or more $M_w 6.2+$ natural events in a row. (Omerbashich, 2016)

Here I report a reliable detection of the full range of the said 3-day Earth phase's all 72 superharmonic resonance periods ($^{72}/_{72}$ h, $^{72}/_{71}$ h, ... $^{72}/_1$ h) in 866 occurrences of $M_w 5.6+$ between 2015-2019. The spectra were computed in the 55'-15 days band (0.303 mHz–0.771605 μ Hz), and analyzed with respect to the estimated 99% confidence level (7 superharmonic resonance periods), 95% confidence level (17), 89% confidence level (25), or 67% confidence level (23). To the best of author's knowledge, after the subject of mechanical-vibration-induced seismotectonics was abandoned early on, there has been no revisiting it in modern times. Additionally, various studies since the 1950s found no periodicity in earthquakes occurrences (Omerbashich, 2004).

2. Signal

Unlike in linear systems where we are concerned with the forcing period $T \in \mathfrak{R}$ alone, in modeling the resonant response of a nonlinear system such as the Earth, besides the forcer, we must also consider additional vibration

$$\frac{n}{m} \cdot \frac{1}{T}; \quad n \in \mathfrak{N} \quad (1)$$

called *subharmonic oscillation* when:

$$0 < \frac{n}{m} < 1; \quad n > 1 \wedge n \in \mathfrak{N}, \quad (2)$$

or *superharmonic oscillation* when:

$$\frac{n}{m} > 1; \quad \frac{n}{m} \in \mathfrak{R}. \quad (3)$$

As seen from Eqns. (1)–(3), $n > 1$ is always a positive integer number and $n / m > 1$ a positive number but not necessarily an integer. The matching of the natural period of a solid body to the natural period of an overwhelming body or to shorter or longer fractional multiple periods is called resonance. Thus, matching can be harmonic and it is called simply *mechanical resonance* when natural periods of two bodies match, a *subharmonic resonance* when one body's natural period matches another body's subharmonic period or its fractional multiple, Eqns. (1) and (2), and a *superharmonic resonance* when one body's natural period matches another body's superharmonic period or a fractional multiple, Eqns. (1) and (3).

Subharmonic and superharmonic resonances can arise in discrete regions of a physical system. As with all solids, tectonic plates and upper mantle's brittle regions are the vibrating parts of the Earth. As based on resonance research from mechanical and electrical engineering, while the former type of resonance mostly occurs at periods shorter than (usually: fractions of) the long-periodic excitation, the latter type mostly occurs at periods that are longer than (usually: integer multiples of) the long-periodic excitation. Most nonlinear systems and nonlinearity models exhibit only the simplest n / T superharmonic periods as the special case $m = 1$. Also, it can be shown that a linear-system resonator is just a special case of a subharmonic resonator. (Yang & al., 2016)

Past spectral analyses of earthquake data searching for a resonance signal under the assumptions of the Earth's linearity or simple nonlinearity bore no fruit. Therefore, of interest here is a strictly nonlinear, subharmonic and superharmonic signal T_{Rsup} , as the only unexplored path. This necessitates looking into the long-periodic band, which then here starts at the Earth's natural period, encompasses the phase forcer, and ends at the lunar-synodic half-month period. Note lunar forcing is a rather crucial part of signal instead of noise as claimed classically.

To that end, I consider the Earth under nonlinear forcing, as prescribed by the georesonator hypothesis. Note that, for nonlinear components of the resonance to occur, it does not matter where this nonlinearity originates – in the source mechanism, in the damping, or in both (Den Hartog, 1985). Importantly then for an approach to modeling the Earth as a fully nonlinear forced system (when one could expect anything): a single excitation always induces superharmonic resonances only. (Yang & al., 2016). No mathematical solution for predicting superharmonic resonance in a nonlinear system exists, so one is confined to data analysis in the trial-and-error approach. Studying of superharmonic resonance and vibrational resonance in nonlinear physical systems, in general, has only started picking up the pace in recent decades.

3. Data analysis

The analyzed data represented the Earth's strong seismicity sampled at 1Hz rate, in moment magnitudes M_w as the most realistic (physics-based) representation of seismicity (Kanamori, 1977) (Dziewonski & al., 1981). The data consisted of occurrences of all $q = 866$ earthquakes of $M_w 5.6+$ to within 10^{-1} , spanning $\Delta t = 1211$ days from 01 October 2015–02 February 2019; see Table 1. The robust (outliers M^{**} discarded) means from the USGS, EMSC, and GFZ moment magnitudes were spectrally analyzed, as:

$$\overline{M}_i|_{i=1}^q = \frac{1}{3} [M_i^{USGS} + M_i^{EMSC} + M_i^{GFZ}]; \quad i \in \aleph \wedge \overline{M}_i|_{i=1}^q \Leftrightarrow M_i \neq M^{**}, \quad (4)$$

Here I tacitly assume that any events in excess to what the above hypothesis prescribes to be sufficient for a valid description of the proposed mechanism of resonance seismotectonics, in fact, overrepresent rather than enrich the data. Hence to prepare data, I eliminated redundancy by excluding 21 events that had occurred within minutes and location of another, stronger event that I have kept; see Table 4. Another tacitly made assumption was that all spectral estimates at different confidence levels are physically meaningful if at least 67% reliable. Then spectral values were analyzed together regardless of the associated confidence level. Parts of the herein reported analyses justify such an approach, e.g., detection of the known physical processes such as the clustering of Earth natural mode's period estimates that never fall below 89% confidence, thus indicating a physical process.

The spectra were computed using the Gauss-Vaniček spectral analysis (GVSA) technique (Vaníček, 1969) (Vaníček, 1971), with $k = 1000$ spectral resolution:

$$s_j^{GVSA}(T_j, M_j^{GVSA}); j = 1 \dots k \wedge k \in \mathbb{N}. \quad (5)$$

The GVSA falls in the Least Squares Spectral Analysis class of spectral methods which fit data with trigonometric functions. The GVSA offers numerous advantages over the Fourier class of spectral analysis methods (FSA), particularly in analyzing raw records of unevenly spaced real data (Press & al., 2007). Application of GVSA is undemanding, with little to no data preprocessing and no postprocessing required. Since variance-based, GVSA provides a straightforward statistical analysis with a generally linear depiction of background noise levels, of accuracy generally unattainable with FSA due to the way data are treated from the outset and in their entirety. The significantly complete modeling of noise makes GVSA more reliable than FSA, as the latter merely unveils periodicity in data that are presumed fit and undistorted. (Omerbashich, 2004) (Omerbashich, 2006b). GVSA is one of the most accurate methods of numerical analysis (Omerbashich, 2019).

As desired, the data preparation, Table 3, has boosted the magnitude of the absolutely highest spectral peak (that of the 1h period), from 2.2 to 2.3 var%. At the same time, the removal did not affect estimates of spectral periods, while causing an average change in spectral magnitudes, of $\Delta s < 0.04$ var% (with just two outliers reaching ± 0.2 var%), but this change is well below the spectral magnitude precision of 10^{-1} and therefore of no concern either. In addition, the removal has somewhat boosted 491 spectral peaks but also somewhat reduced 509, out of the total spectral resolution of $k = 1000$ peaks, regardless of significance regime. Most importantly, the removal has increased estimates of confidence levels as well, but only up to $\frac{1}{2}$ of the declared spectral magnitudes precision, of 0.1 var%. This, as follows: from 1.06 to 1.09 var% for 99%, from 0.69 to 0.71 var% for 95%, and from 0.47 to 0.52 var% for 89%, while the 69% confidence-level estimates (which normally make majority in all of the spectra) remained the same, at 0.26 var%. The tradeoff of the removal in terms of disturbed confidence (i.e., the number of spectral peaks either lost or gained with respect to a specific confidence level) was around: 2% gain for 67% level, 12% loss for 89%, 4% loss for 95%, and 7% loss for 99%. The absolute end-result of this post-removal shuffling of significance levels has driven only 12 of all 219 periods with 67%-confidence to drop below significance, out of the total of 385 (across 4000 spectral points of computing the spectrum; in all four significance regimes: 107 at 89%, 46 at 95%, 13 at 99%) that were significant before the removal. (Note here that most of the 67%-confident peaks clustered.)

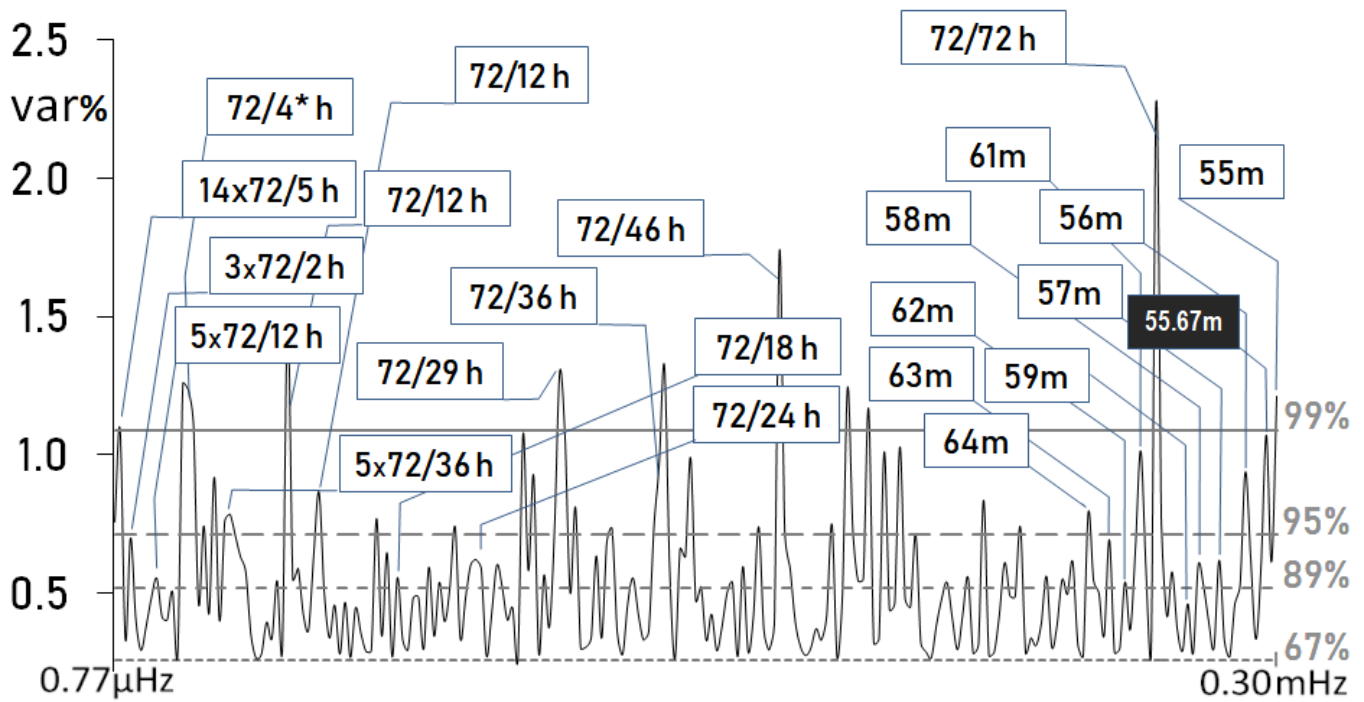


Figure 2. The spectrum of significant periods in 845 occurrences of $M_w5.6+$ earthquakes between 1 October 2015 and 2 February 2019, Eqn. (4). Significance levels: 67% (dotted line), 89% (dashed line), 95% (em-dashed line), and 99% (solid line). Spectral magnitudes are in percentage variance (var%). Corresponding spectral values are in Tables 2 & 4. Omitted events listed in Table 3. Labels non-arbitrary. The highlighted label marks the proposed period of self-excited oscillation of the Earth; see Discussion section. A * marks a value obtained as a simple average of two neighboring doublets of a split period (mode doublet). For example, the 18 h period, Table 2, was obtained as 17.99954 h, or a simple average of the 99%-significant periods of 66702.31181 s (with very high fidelity, of $\Phi = 21$) and 62894.39540 s (with a very fidelity, of $\Phi = 19$). In statistics, an estimated value with $\Phi \geq 12$ usually is considered significant of its own and as system-based (here: as having a physical meaning). The 0.30mHz cutoff was selected as the free-to-forced oscillation natural boundary.

Therefore, based on the analyses, the removal was overall beneficial. It enhanced the absolutely highest peak's estimate while not affecting computations of periods or estimates of significances. The 4% boost in the magnitude of the absolutely highest spectral peak after the data removal was not alone; in fact, the second- and third-highest peaks also got considerably boosted, up to 4%; see Table 5. All spectral computations and confidence-level estimates reflect this benefit that justifies the removal procedure as physically meaningful, even for datasets unsusceptible to a 2% refinement as done here.

Suppose the starting physical hypothesis on resonance tectonics correct tacitly, and therefore the removal procedure justified from a physical point of view in general and not just for the herein analyzed data. It then follows from the above that the data indeed possess a high degree of internal consistency and robustness as well as ambiguity – just as one would expect from data which describe a constantly but inconsistently driven physical process. The data indeed described a genuine even though non-linear behavior of a physical system, as could be grasped already from Figure 5. While faithfully representing the hypothesized physical mechanism, robustness and consistency of the data also justify the choice of $M_w5.6$ as the cutoff magnitude and a good approximation of the lower defining boundary of the mechanism's contribution to the Earth's energy budget.

Since small, short-periodic excitations, usually mean a strong response in the corresponding long-periodic band, I also computed spectra in the 2s-55' band. Those spectra indeed showed no significant response beyond geophysical noise at 67% confidence (as confirmed by computed spectral fidelity of $\Phi = 0$ throughout), corroborating that the spectra in the primary band of interest, 55'-15 days, describe the culprit behind strong seismicity and tectonics. Similarly, the 2s-55' spectra thus indicate that $M_w5.6+$ earthquake occurrences are useless for studying the Earth's deep interior and inner core. Also looked into are the following spectral bands: 1-605 days, 3-180 days, 30'-605 days, 50'-10 days, 30'-10 days, 30'-300 days, 30'-303 days, 45'-15 days, 50'-15 days, 55'-7 days, 55'-10 days, 55'-14 days, 55'-20 days, 55'-22 days, 55'-30 days. However, those bands did not contain meaningful results.

0.0	5.5	11097118.0	5.9	21061756.0	6.0	32221122.0	5.9	39950978.0	5.7
57741.0	6.1	11199149.0	6.1	21064898.0	6.1	32341235.0	5.9	40062032.0	5.8
334022.0	6.0	11262597.0	6.0	21116029.0	5.8	32369395.0	6.6	40132292.0	5.9
614223.0	5.8	11516117.0	5.8	21312213.0	5.7	32454800.0	5.6	40176716.0	5.9
717749.0	6.0	11655658.0	5.9	21444798.0	6.2	32477390.0	5.6	40267086.0	5.7
910557.0	7.1	11783560.0	5.8	21731412.0	5.7	32559077.0	6.2	40399690.0	6.5
1097040.0	6.1	12141218.0	6.1	21803617.0	5.7	32786960.0	5.8	40592058.0	7.9
1105692.0	6.0	12455622.0	7.8	21862276.0	6.3	32944437.0	5.8	41234625.0	5.9
1170437.0	5.7	12574304.0	5.8	21927288.0	5.9	32991824.0	6.0	41351958.0	5.9
1317771.0	5.7	12948021.0	6.0	22059029.0	6.1	33042122.0	6.1	41684297.0	5.7
1383206.0	7.5	13338639.0	6.3	22061762.0	6.3	33088905.0	5.8	42037669.0	6.2
1597835.0	5.8	13530574.0	5.7	22248564.0	5.8	33101832.0	5.9	42268057.0	6.5
1923610.0	5.9	13883946.0	6.0	22472465.0	6.4	33133009.0	6.0	42952449.0	6.4
1984768.0	5.8	13919425.0	6.0	22686641.0	5.8	33165051.0	5.9	43218778.0	6.5
2141289.0	6.5	14046854.0	6.4	22818868.0	5.9	33217603.0	5.8	43428971.0	5.9
2414137.0	6.8	14104366.0	5.6	23156974.0	5.8	33342253.0	6.5	43489958.0	6.9
2426257.0	5.7	14495298.0	5.7	23299552.0	5.8	33559643.0	6.0	43512639.0	5.9
2507932.0	5.7	14634325.0	5.8	23690747.0	5.8	33809078.0	6.3	43800776.0	5.7
2533855.0	6.5	14717930.0	5.6	23690915.0	5.9	34086919.0	5.7	44128938.0	6.0
2617659.0	6.4	15010981.0	5.9	23735105.0	5.9	34107199.0	5.8	44205132.0	5.7
2739512.0	6.8	15071330.0	6.1	23735700.0	6.3	34113580.0	6.0	44249171.0	5.7
2817613.0	5.8	15108834.0	6.2	23943652.0	6.0	34235693.0	5.9	44286707.0	6.3
2980531.0	6.7	15204468.0	6.9	23944507.0	6.3	34313283.0	5.8	44435533.0	5.7
3061455.0	5.7	15377596.0	5.9	23944946.0	5.9	34433215.0	6.1	44590700.0	5.9
3167007.0	5.8	15458327.0	5.7	23947699.0	5.8	34499985.0	5.9	44992510.0	6.0
3225189.0	5.9	15458563.0	6.7	24438154.0	5.8	34567612.0	7.8	45036454.0	5.7
3276843.0	6.5	15462091.0	6.0	24560231.0	6.0	34569362.0	6.4	45470840.0	6.0
3404098.0	7.0	15486568.0	6.0	24768255.0	5.8	34570599.0	6.1	46144453.0	6.2
3629408.0	6.1	15532608.0	6.6	24837197.0	5.9	34576521.0	6.2	46293198.0	6.6
3748799.0	5.7	15787110.0	5.7	24902086.0	5.8	34578295.0	5.8	46333160.0	5.7
3903930.0	6.0	15804918.0	5.6	24969744.0	5.8	34597972.0	5.7	46773852.0	6.5
3938088.0	7.6	15816772.0	6.6	25000244.0	6.1	34616296.0	6.4	46905186.0	6.1
4049352.0	6.7	15964001.0	5.8	25008159.0	6.4	34788865.0	5.8	47168000.0	5.9
4190656.0	6.2	16088351.0	6.9	25044794.0	5.9	34841646.0	5.7	47317668.0	5.7
4211701.0	5.9	16104349.0	5.9	25052894.0	5.7	35208098.0	6.4	47353365.0	5.8
4355804.0	5.9	16135803.0	5.8	25115346.0	5.9	35294623.0	6.9	47454370.0	5.7
4522340.0	5.8	16168859.0	5.9	25359743.0	7.7	35306616.0	5.9	47478295.0	5.8
4800528.0	7.1	16169430.0	6.1	25497436.0	5.8	35427832.0	5.8	47635788.0	5.8
5007241.0	7.2	16170382.0	5.6	25570004.0	5.7	35468851.0	5.8	47777017.0	6.3
5189145.0	6.8	16178862.0	6.0	25852745.0	6.2	35545662.0	6.9	47928324.0	5.7
5198515.0	6.0	16203261.0	6.3	25860508.0	6.3	35616504.0	6.6	48068142.0	6.0
5281749.0	5.7	16208344.0	5.6	26497829.0	7.1	36164660.0	6.2	48070429.0	5.9
5914428.0	6.5	16262123.0	6.1	26505203.0	6.1	36289649.0	5.9	48447600.0	6.0
6023688.0	6.0	16270140.0	7.0	26705950.0	5.8	36361681.0	5.7	48602544.0	6.9
6085738.0	5.8	16271281.0	5.7	27027243.0	5.7	36433018.0	6.3	48837027.0	5.7
6169890.0	6.0	16271390.0	5.7	27076418.0	6.0	36593176.0	5.9	48926040.0	5.9
6422344.0	5.8	16383751.0	7.8	27124577.0	7.4	36594447.0	6.5	48943633.0	6.8
6518877.0	6.1	16409873.0	5.7	27160655.0	5.8	36706738.0	6.0	49001787.0	5.7
6531292.0	5.8	16410894.0	5.9	27216320.0	6.0	36741221.0	6.6	49174548.0	6.2
6598919.0	5.7	16517405.0	5.9	27241318.0	5.8	36751361.0	7.8	49180931.0	6.3
6603521.0	6.3	16576175.0	6.2	27283757.0	6.1	36766346.0	5.9	49270456.0	5.9
6886538.0	5.8	16673861.0	6.1	27513818.0	6.0	36766801.0	6.5	49319467.0	6.0
7092054.0	5.8	16673944.0	6.0	27535227.0	6.2	36843240.0	6.9	49493610.0	5.8
7146274.0	6.3	16687419.0	5.8	27567529.0	6.8	36845238.0	5.9	49562402.0	5.9
7193169.0	5.8	16826855.0	6.1	27579159.0	5.7	36852136.0	5.8	49790120.0	5.7
7241173.0	5.8	16827847.0	5.9	27677317.0	5.9	36870574.0	5.8	49791084.0	5.9
7394954.0	6.7	16907308.0	5.7	27977632.0	7.1	36919710.0	6.0	49795481.0	6.2
7493107.0	5.9	17069308.0	5.7	28145730.0	6.7	36999426.0	5.8	49827489.0	6.0
7519089.0	6.0	17100663.0	6.0	28213709.0	5.8	37213516.0	6.0	49870566.0	6.8
7563824.0	5.7	17177026.0	5.6	28280512.0	7.0	37504504.0	7.9	49935831.0	5.8
7748155.0	5.6	17294116.0	6.0	28282679.0	6.0	37506693.0	6.4	49991250.0	6.5
7960557.0	5.7	17404640.0	7.0	28436798.0	5.7	37513588.0	6.7	49997617.0	5.7
8062920.0	6.5	17426252.0	6.6	28489326.0	5.7	37572619.0	5.9	50049907.0	5.7
8064717.0	6.2	17537977.0	5.8	28621376.0	5.8	37575817.0	5.9	50118319.0	6.2
8124545.0	5.9	17695518.0	5.7	28648679.0	6.1	37587058.0	6.2	50323697.0	5.7
8161734.0	5.7	17766285.0	5.7	28903814.0	6.1	37600445.0	6.4	50387192.0	6.2
8197195.0	5.8	17905219.0	5.7	29034734.0	6.1	37740322.0	6.4	50775008.0	5.9
8274561.0	6.1	18225476.0	5.8	29043087.0	5.8	37769829.0	6.0	50835761.0	5.7
8274568.0	6.6	18555670.0	5.8	29195748.0	5.8	37812070.0	6.7	51149651.0	5.7
8302096.0	5.7	18782700.0	5.8	29350945.0	5.9	37871272.0	5.9	51176395.0	5.8
8674100.0	5.9	18891947.0	5.8	29370534.0	6.0	38075770.0	5.9	51601157.0	6.6
8842628.0	5.9	19090859.0	6.7	29451678.0	5.7	38084569.0	5.8	51602508.0	5.8
8932252.0	6.5	19122638.0	6.9	29607851.0	6.0	38208380.0	7.6	51676425.0	5.7
9164064.0	7.1	19300678.0	6.0	29612152.0	5.8	38461366.0	5.9	51974921.0	6.8
9212644.0	5.7	19853303.0	5.9	29715690.0	5.7	38583253.0	6.2	51979932.0	5.7
9228356.0	6.3	19854758.0	6.4	29921110.0	6.1	38848621.0	5.8	52050088.0	6.0
9310457.0	6.0	19946564.0	6.9	30122308.0	6.3	38884750.0	5.9	52605968.0	5.7
9440113.0	5.7	19961453.0	7.2	30203823.0	6.3	38895463.0	5.9	52755545.0	5.7
9656944.0	7.2	20204861.0	6.3	30247703.0	5.9	38895477.0	6.3	52803153.0	6.3
9794575.0	6.0	20221673.0	5.9	30283868.0	6.4	39012985.0	6.9	52932574.0	5.8
9885879.0	6.2	20260516.0	5.7	30285155.0	6.9	39015846.0	6.0	52957979.0	6.9
9955396.0	5.7	20354396.0	6.4	30399832.0	5.6	39092867.0	5.7	53019011.0	5.9
10234881.0	6.4	20366821.0	5.7	31122281.0	5.7	39216869.0	5.7	53059570.0	5.8
10343249.0	5.8	20638504.0	5.7	31233454.0	5.7	39398162.0	5.9	53174482.0	5.7
10480989.0	6.4	20676567.0	6.3	31301754.0	5.7	39451866.0	6.0	53270996.0	6.1
10597019.0	6.3	20713161.0	6.0	31488313.0	5.7	39561461.0	7.3	53396377.0	5.8
10803978.0	6.2	20829332.0	6.3	31557021.0	5.8	39594669.0	6.3	53667298.0	6.8
10941457.0	5.8	20859550.0	6.3	31775118.0	5.7	39704532.0	5.8	53853186.0	5.7
11006000.0	5.7	20907334.0	5.8	32051252.0	6.3	39858199.0	5.7	53945184.0	6.0
11081187.0	6.0	20978222.0	6.1	32217532.0	6.8	39906935.0	6.0	54206687.0	6.0

54252424.0 6.0	65035671.0 6.6	75166252.0 5.9	88350691.0 6.4	96633255.0 5.8
54319132.0 5.9	65318654.0 6.8	75178802.0 5.8	88854888.0 5.8	96643425.0 6.2
54394418.0 6.0	65337171.0 5.7	75184729.0 6.1	89002231.0 6.9	96689109.0 6.0
54522165.0 5.8	65577934.0 5.7	75190913.0 6.3	89182864.0 5.7	96850763.0 6.0
54716993.0 5.9	65622633.0 6.5	75244986.0 5.7	89324966.0 5.9	96892198.0 5.9
54855251.0 5.8	65659145.0 5.7	75285197.0 6.0	89457360.0 5.9	97260814.0 6.8
54860871.0 6.5	65745965.0 6.0	75318578.0 6.1	89618569.0 6.4	97282726.0 5.7
54931605.0 5.7	65847927.0 5.8	75489846.0 5.9	89641136.0 6.0	97371432.0 6.1
55031493.0 5.7	65893209.0 6.1	75706635.0 5.7	89750026.0 6.1	97477674.0 6.3
55183544.0 5.8	66043331.0 7.3	75726012.0 6.0	89902849.0 6.6	97763145.0 6.1
55289042.0 6.6	66058081.0 5.9	75878221.0 6.7	89976325.0 5.8	97844776.0 6.4
55421521.0 5.9	66072737.0 6.6	75930246.0 5.9	89976407.0 6.2	97855975.0 6.3
55449603.0 6.4	66238107.0 5.8	76063427.0 6.8	90052736.0 6.5	97871449.0 6.1
55653375.0 5.9	66348392.0 5.9	76126203.0 5.8	90080780.0 6.1	98105379.0 6.7
55787070.0 5.7	66358050.0 5.8	76145237.0 5.7	90170612.0 8.2	98435459.0 5.9
55822143.0 6.3	66490694.0 6.4	76250970.0 5.9	90184457.0 6.3	98635593.0 5.8
55867089.0 7.7	66553856.0 5.8	76798443.0 5.7	90185573.0 6.8	98649885.0 6.0
55876153.0 6.4	66616181.0 6.3	77423246.0 6.3	90223222.0 6.9	98696486.0 6.2
55999219.0 6.0	66636777.0 6.6	77454147.0 6.1	90419738.0 7.3	98722878.0 5.7
56042119.0 5.8	66640321.0 5.9	77500926.0 5.7	90423382.0 6.5	98852842.0 5.7
56122505.0 6.6	66664044.0 7.0	77521278.0 5.7	90462941.0 6.2	98865914.0 5.7
56597811.0 5.9	66669198.0 6.0	77541522.0 6.4	90477103.0 5.8	99055539.0 5.8
56689952.0 5.8	66736501.0 6.0	77590495.0 6.7	90496411.0 5.8	99131602.0 7.0
56710639.0 5.9	67163636.0 5.8	77882106.0 5.8	90527950.0 6.3	99203475.0 6.4
56981083.0 5.7	67299306.0 6.0	77891371.0 6.9	90634080.0 7.1	99516122.0 7.5
57425675.0 5.8	67469580.0 5.7	77896687.0 5.7	90748438.0 5.9	99524822.0 6.6
57511144.0 5.7	67556204.0 6.5	78181287.0 6.1	90767840.0 6.0	99671453.0 5.9
57619837.0 5.8	67628200.0 6.1	78209068.0 6.8	90972724.0 6.2	100027825.0 7.1
57640565.0 5.7	67629234.0 6.0	78244034.0 5.9	90994385.0 5.7	100153070.0 6.3
57731024.0 6.5	67832580.0 6.1	78433055.0 6.0	91028347.0 6.4	100485991.0 6.1
57767507.0 6.3	67878719.0 5.7	78451913.0 5.8	91038530.0 5.8	100503014.0 5.8
57961941.0 6.2	68225208.0 6.4	78612753.0 6.3	91047350.0 7.1	100716094.0 6.3
58075087.0 5.8	68231632.0 5.9	78737786.0 5.7	91550472.0 5.9	100788102.0 5.8
58126327.0 6.4	68259302.0 6.3	78765890.0 5.7	91703513.0 6.6	100857949.0 7.3
58175718.0 5.7	68309166.0 5.7	78888208.0 6.2	91781591.0 7.8	100906667.0 5.9
58309542.0 5.7	68365099.0 6.1	79353278.0 5.9	91818958.0 6.2	101021335.0 6.0
58420519.0 5.7	68522034.0 5.7	79704791.0 6.0	91820591.0 5.8	101126176.0 5.7
58557796.0 6.6	68600831.0 6.0	79872490.0 5.8	91923643.0 6.1	101139157.0 6.4
58640686.0 6.4	68647525.0 6.0	79948990.0 5.7	91933603.0 5.8	101187913.0 6.1
59340104.0 6.3	68720857.0 6.5	80573220.0 5.8	92054130.0 6.5	101366111.0 5.8
59731850.0 6.3	68889113.0 6.5	80645327.0 5.8	92085775.0 6.9	101498847.0 5.8
60045093.0 6.1	69357852.0 5.8	80727572.0 5.9	92140533.0 6.3	101587381.0 7.0
60337844.0 6.1	70014255.0 5.7	80736708.0 5.9	92472850.0 5.8	101691786.0 5.7
60378795.0 8.1	70115087.0 5.7	80775403.0 6.0	92502735.0 5.7	101756371.0 6.0
60545479.0 5.8	70124391.0 5.7	81005810.0 6.9	92664943.0 6.5	102246664.0 5.9
60612255.0 5.8	70437673.0 5.9	81033778.0 6.1	92788295.0 6.0	102248972.0 6.8
60683943.0 5.7	70988988.0 5.8	81385309.0 6.0	92804506.0 5.8	102261487.0 5.8
60943523.0 5.8	71085326.0 7.5	81395139.0 6.2	93033873.0 5.8	102314752.0 5.7
61191002.0 5.7	71227818.0 6.0	81486050.0 5.7	93033935.0 5.8	102328273.0 6.6
61275053.0 5.8	71375310.0 5.8	81507983.0 5.9	93214565.0 5.8	102483805.0 6.3
61377512.0 7.1	71454159.0 7.1	81931923.0 5.9	93454887.0 5.8	102672273.0 5.8
61404444.0 6.1	71647667.0 5.9	82023968.0 5.8	93576581.0 5.7	103108222.0 6.6
61458070.0 6.1	71665272.0 5.9	82115164.0 5.7	93650635.0 6.1	103115234.0 5.7
61470824.0 6.4	71762452.0 5.8	82126026.0 5.7	93661598.0 7.5	103270230.0 6.2
61478250.0 5.9	71809967.0 5.8	82140565.0 6.1	93837377.0 6.6	103350145.0 6.0
61484598.0 5.7	71911300.0 6.3	82481400.0 5.7	93971015.0 6.0	103362276.0 5.9
61642449.0 5.7	72029435.0 6.3	83473022.0 5.9	94284218.0 5.7	103480605.0 6.7
61695721.0 5.8	72221929.0 6.0	83489577.0 5.7	94403638.0 5.7	103567229.0 5.7
61703816.0 6.1	72232537.0 7.9	83519523.0 5.7	94403745.0 5.9	103604472.0 5.7
61732263.0 5.7	72323715.0 6.3	84377543.0 5.9	94603747.0 6.1	103647796.0 6.0
61780206.0 5.7	72375592.0 5.8	84652046.0 6.0	94729729.0 6.0	103666437.0 6.4
61903998.0 5.9	72378868.0 6.2	84838415.0 5.8	94737134.0 7.0	103716338.0 6.7
61932234.0 6.4	72409508.0 5.8	85129914.0 5.7	94745996.0 6.5	103924155.0 5.7
61989966.0 5.8	72431018.0 5.8	85148246.0 6.1	94911223.0 5.7	104001076.0 5.7
62595779.0 5.7	72539512.0 6.3	85398457.0 5.9	94922259.0 5.7	104007332.0 6.2
62809407.0 6.2	72688019.0 6.5	85863644.0 5.9	94961656.0 6.7	104023002.0 5.9
62844320.0 5.7	72915054.0 6.2	86373842.0 6.1	95026169.0 5.7	104065238.0 6.2
63004114.0 6.1	73015785.0 6.0	86495264.0 5.8	95053508.0 5.9	104116821.0 5.8
63028373.0 6.2	73104107.0 5.8	86531863.0 6.0	95184456.0 6.5	104394928.0 5.9
63034707.0 6.5	73285236.0 6.1	87007842.0 6.4	95618671.0 6.0	104570286.0 6.5
63149774.0 6.3	73464877.0 6.4	87152473.0 6.0	95721623.0 6.8	104632289.0 6.1
63194248.0 6.7	73709269.0 5.9	87192790.0 6.0	95801932.0 5.8	
63860693.0 6.1	73717783.0 5.8	87279190.0 5.8	95843279.0 5.7	
63936355.0 5.9	73835683.0 5.8	87343607.0 5.9	96025205.0 5.7	
64280187.0 5.9	73923488.0 6.0	87539747.0 5.8	96040726.0 6.8	
64374701.0 6.7	74016937.0 5.8	87542422.0 5.8	96077373.0 5.9	
64740000.0 5.8	74020018.0 5.7	87557667.0 6.0	96298067.0 6.1	
64750496.0 5.9	74357014.0 7.2	87739213.0 5.9	96328695.0 6.3	
64943163.0 6.8	74360446.0 5.8	87786681.0 5.8	96388202.0 5.8	
64949080.0 5.9	74556055.0 5.9	87874794.0 5.9	96398253.0 6.1	
64983285.0 6.1	75113317.0 7.5	88330277.0 6.0	96444955.0 5.7	

TABLE 1

845 OCCURRENCES OF
Mw5.6+ EVENTS FROM
1 OCT 2015 UNTIL 2
FEB 2019. OMITTED
EVENTS IN TABLE 3.

Superharmonic resonance period (h)					Superharmonic resonance period (h)				
fractional	theoretical	detected	difference	$\delta\sigma$	fractional	theoretical	detected	difference	$\delta\sigma$
72/1*	72.0000	75.0591	-3.0591	0.4994	72/37	1.9459	1.9636	-0.0177	0.0082
72/2	36.0000	33.3241	2.6759	0.3420	72/38	1.8947	1.8831	0.0116	0.0077
72/3	24.0000	23.2132	0.7868	0.1308	72/39	1.8462	1.8305	0.0157	0.0076
72/4*	18.0000	17.9995	0.0005	0.0914	72/40	1.8000	1.8160	-0.0160	0.0073
72/5	14.4000	14.4466	-0.0466	0.0921	72/41	1.7561	1.7536	0.0025	0.0067
72/6	12.0000	12.6545	-0.6545	0.0926	72/42	1.7143	1.7016	0.0127	0.0068
72/7	10.2857	10.0282	0.2575	0.0450	72/43	1.6744	1.6646	0.0098	0.0066
72/8	9.0000	8.8661	0.1339	0.0329	72/44*	1.6364	1.6351	0.0013	0.0065
72/9	8.0000	7.8772	0.1228	0.0288	72/45	1.6000	1.5869	0.0131	0.0066
72/10	7.2000	7.1419	0.0581	0.0247	72/46	1.5652	1.5573	0.0079	0.0063
72/11	6.5455	6.5321	0.0134	0.0238	72/47	1.5319	1.5416	-0.0097	0.0062
72/12	6.0000	6.0183	-0.0183	0.0240	72/48	1.5000	1.5062	-0.0062	0.0060
72/13	5.5385	5.6132	-0.0747	0.0240	72/49	1.4694	1.4676	0.0018	0.0060
72/14	5.1429	5.1709	-0.0280	0.0221	72/50	1.4400	1.4468	-0.0068	0.0061
72/15	4.8000	4.7434	0.0566	0.0219	72/51	1.4118	1.4091	0.0027	0.0060
72/16	4.5000	4.6008	-0.1008	0.0209	72/52	1.3846	1.3941	-0.0095	0.0062
72/17	4.2353	4.2008	0.0345	0.0158	72/53	1.3585	1.3590	-0.0005	0.0058
72/18	4.0000	3.9650	0.0350	0.0154	72/54	1.3333	1.3412	-0.0079	0.0060
72/19	3.7895	3.7696	0.0199	0.0149	72/55	1.3091	1.2939	0.0152	0.0057
72/20	3.6000	3.5236	0.0764	0.0148	72/56	1.2857	1.2741	0.0116	0.0048
72/21	3.4286	3.4443	-0.0157	0.0106	72/57	1.2632	1.2636	-0.0004	0.0041
72/22	3.2727	3.2842	-0.0115	0.0105	72/58	1.2414	1.2381	0.0033	0.0042
72/23	3.1304	3.1275	0.0029	0.0104	72/59*	1.2203	1.2103	0.0100	0.0043
72/24	3.0000	2.9949	0.0051	0.0105	72/60	1.2000	1.2008	-0.0008	0.0034
72/25	2.8800	2.8821	-0.0021	0.0106	72/61	1.1803	1.1762	0.0041	0.0036
72/26	2.7692	2.7691	0.0001	0.0107	72/62	1.1613	1.1628	-0.0015	0.0035
72/27	2.6667	2.6569	0.0098	0.0109	72/63	1.1429	1.1425	0.0004	0.0037
72/28	2.5714	2.5821	-0.0107	0.0109	72/64	1.1250	1.1299	-0.0049	0.0039
72/29	2.4828	2.4911	-0.0083	0.0109	72/65	1.1077	1.1107	-0.0030	0.0038
72/30	2.4000	2.4317	-0.0317	0.0109	72/66	1.0909	1.0909	0.0000	0.0039
72/31	2.3226	2.3269	-0.0043	0.0098	72/67	1.0746	1.0693	0.0053	0.0042
72/32	2.2500	2.2580	-0.0080	0.0098	72/68	1.0588	1.0546	0.0042	0.0039
72/33	2.1818	2.1524	0.0294	0.0098	72/69	1.0435	1.0438	-0.0003	0.0031
72/34	2.1176	2.1274	-0.0098	0.0089	72/70	1.0286	1.0321	-0.0035	0.0036
72/35	2.0571	2.0514	0.0057	0.0088	72/71	1.0141	1.0195	-0.0054	0.0050
72/36	2.0000	1.9763	0.0237	0.0089	72/72	1.0000	0.9984	0.0016	

*) the value obtained as a simple average of two detected doublets of a split period (mode doublet).

99% (7)
95% (17)
89% (25)
67% (23)

Table 2. Detected superharmonic resonance; deviation divergence (Figure 6b); and confidence.

Event	Date	Time GMT	USGS	EMSC	GFZ	$\overline{M_w}$	d (km)	Location
01	21 Dec 2018	08:30:16	5.7	5.7	5.7	5.7	22	Papua New Guinea
02	30 Nov 2018	17:35:37	5.8	5.7		5.7	46	Alaska
03	29 Oct 2018	21:07:13	5.7		5.6	5.7	25	Drake Passage
04	29 Oct 2018	20:17:23	5.8	5.8	5.8	5.8	28	Drake Passage
05	22 Oct 2018	06:22:48	6.5	6.5	6.5	6.5	14	Canada
06	22 Oct 2018	05:39:40	6.5	6.6	6.5	6.5	22	Canada
07	16 Oct 2018	00:28:10	6.3	6.3	6.3	6.3	16	Loyalty Isles
08	10 Oct 2018	22:00:34	6.2	6.2	6.2	6.2	119	Papua New Guinea
09	10 Oct 2018	21:13:16	5.9	5.9	5.9	5.9	28	Papua New Guinea
10	10 Oct 2018	20:59:01	5.9	5.9		5.9	40	Papua New Guinea
11	02 Oct 2018	00:16:43	5.9	5.9	5.8	5.9	19	Indonesia
12	01 Nov 2017	05:09:00	5.9	6.0	5.8	5.9	17	New Caledonia
13	01 Nov 2017	00:09:30	6.1	6.1	6.0	6.1	14	New Caledonia
14	31 Oct 2017	12:37:50	5.7	5.7	5.6	5.7	28	Indonesia
15	31 Oct 2017	11:34:44	5.6	5.7		5.7	36	Indonesia
16	31 Oct 2017	11:31:42	5.8	5.9	5.7	5.8	28	Indonesia
17	28 Oct 2017	16:13:54	5.8	5.8	5.7	5.8	12	Russia
18	28 Apr 2017	16:05:57	5.8	5.9	5.8	5.8	25	Chile
19	24 Nov 2015	22:45:38	7.6	7.6	7.5	7.6	629	Peru
20	11 Nov 2015	02:46:19	6.9	6.8	6.8	6.8	14	Chile
21	07 Nov 2015	07:04:30	6.2	6.0	6.1	6.1	13	Chile

Table 3. The earthquakes omitted from the analysis. Each event listed above belongs both in a time-cluster and a location-cluster of two or more earthquakes Eqn. (4); namely, those that had occurred within minutes-to-hours from each other, as well as at the same location to within 0.1° latitude and longitude. Then only the strongest of the clustering events was used, as it is representative of the resonance magnification that otherwise would have been overrepresented by the discarded events.

Cluster of Earth's natural mode periods in 2015-2019, 845 global occurrences of $M_w \geq 5.6+$ (USGS, EMSC, GFZ)					
theoretical		measured		magnitude	confidence
(s)	(m)	(s)	(m)	var%	%
3300	55	3309.9144	55.17	1.2	99
3360	56	3381.0189	56.35	0.9	95
3420	57	3426.5875	57.11	0.6	89
3480	58	3495.4418	58.26	0.6	89
3540	59	3555.6075	59.26	0.6	89
3600	60	3594.2743	59.90	2.3	99
3660	61	3670.1071	61.17	1.0	95
3720	62	3715.4909	61.92	0.5	89
3780	63	3796.5825	63.28	0.7	89
3840	64	3849.6475	64.16	0.8	95
3900	65	3904.2169	65.07	0.6	89
mean:		60.1498		$\sigma = 3.27$	RSD = 5%

Table 4. The bundled short periods in the 55'-15 days band. Peaks beyond 64' disperse at this end of the band or cluster elsewhere, so they are of no interest. Importantly, the confidence level on the estimates never dropped below 89% across the entire cluster. Note relative standard deviation (RSD) is 5%, which is well within the $\pm 5\%$ declared accuracy of the physical hypothesis that claims to describe the physics responsible for the Earth's seismodynamics. Note also that the natural mode's average period (highlighted row) matches the absolutely strongest spectral peak (which is at the same time cluster-centered) of 0.9984 h, Table 2, to within the 1Hz sampling rate. This strongly suggests that the 72 h forcer is the modulator of the Earth's natural mode via synchronization.

Neither linear detrending nor enforcing (removal of) the lunar-synodic or solar periods proved beneficial, owing to the relatively short data span and external forcing being part of the signal, respectively.

T (s)	T (h)	S_{OR} var%	S_{OR} var%	boost %
3594.274	1.00	2.19	2.28	+4
5606.165	1.56	1.73	1.74	+1
23515.55	6.53	1.45	1.51	+4

Table 5. The response of the three strongest spectral peaks to the 2% removal of overrepresenting data. The spectral peak magnitude estimates are at 99% confidence level, both before and after the data removal.

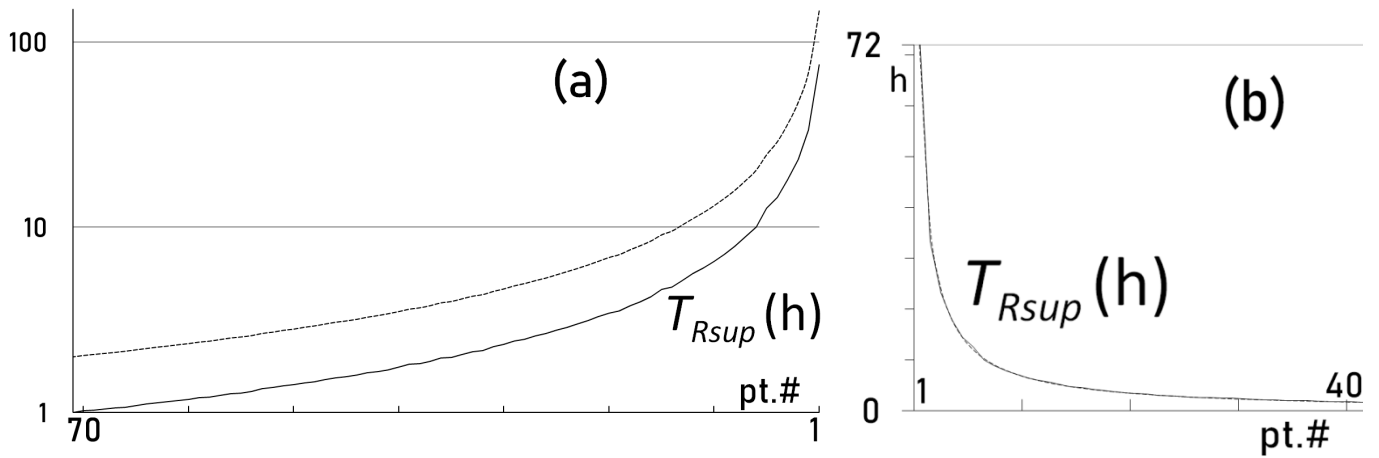


Figure 3. A full range (all 72) of the 3-day phase's theoretical superharmonic-resonance periods: $(72/72)$ h, $(72/71)$ h,... $(72/1)$ h (panel a, dashed line, offset-stacked for legibility against logarithmically-scaled ordinate), v. the corresponding range of the 3-day phase's all 72 significant superharmonic-resonance periods (panel a, solid line). The detected range reveals extreme long-periodic resonance, as a characteristic response of discrete regions of a physical system, in case of the Earth lithosphere chunks and mantle regions. Same in a callout with non-stacked plots, against linearly-scaled ordinate (panel b).

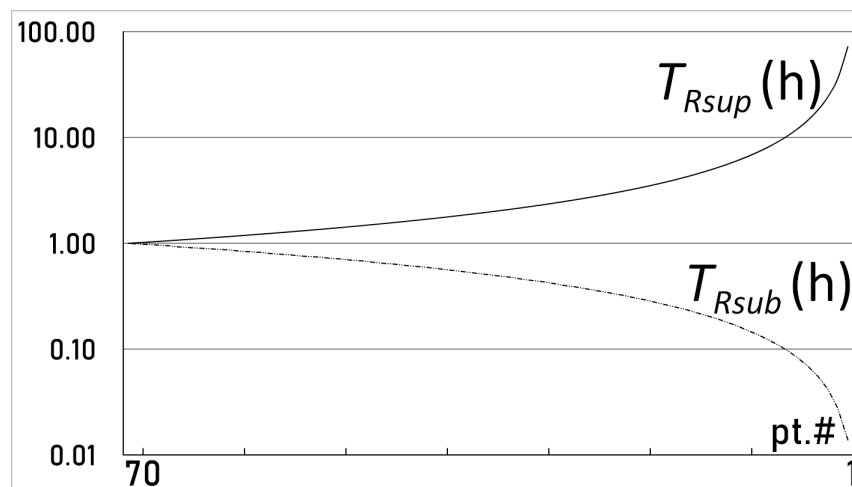


Figure 4. The full range (all 72) of the 3-day phase's theoretical superharmonic-resonance periods: $(72/72)$ h, $(72/71)$ h,... $(72/1)$ h, Figure 3, (solid line), v. the full range of the complementing theoretical subharmonic resonance periods: $(72/72)$ h, $(71/72)$ h,... $(1/72)$ h (dashed line). Abscissa values in reverse-order for legibility.

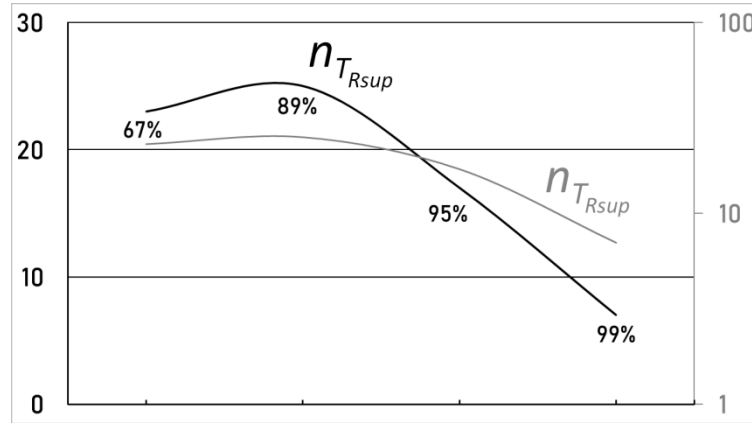


Figure 5. Data quality, as quantified by data responsiveness to estimating significance levels of the detected (range of all) 72 superharmonic resonance periods of the Earth's 3-day phase, Table 2 and Figure 2. The plot indicates a genuine response of a physical system to external forcing at long periods (longer than the system's natural period, estimated by many for the Earth as 57' (Omerbashich, 2004)), because physical data lack detail for theoretical (perfect) data resolution and to secure 99% confidence all the time. Shown are the linear response (dark line) and logarithmic response (light line), in numbers of superharmonic resonance periods per confidence level, Table 2.

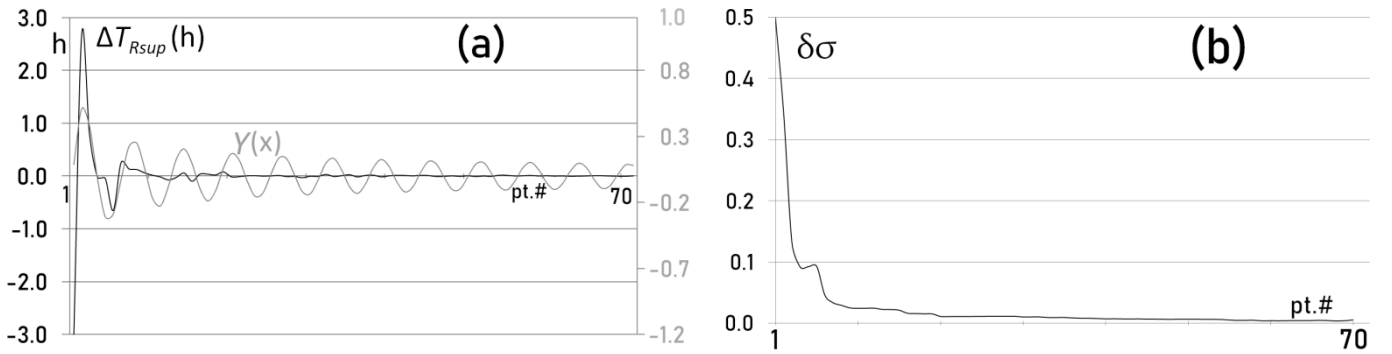


Figure 6. Difference ΔT_{Rsup} in hours (dark line; panel *a*) between the theoretical v. computed resonance periods from the earthquake occurrence spectra that have revealed the Earth's superharmonic resonance, Table 2 and Figure 3. At first sight, the difference seems best modeled by a mother half-wavelet function. But due to the fixed precision of spectral analyses to 10^{-4} or better than 4 s at 1Hz data sampling rate, as well as finiteness of the resonance range and discreteness of the resonating masses, the standard deviation divergence $\delta\sigma$, Table 2, at first changes considerably with lowering the number of differences taken into account, only to stabilize asymptotically rather quickly (panel *b*). So the difference could, in reality, reflect the overall system's response to superharmonic resonance in the form of the Bessel equation (light line; panel *a*), specifically an asymptotically fast-converging Weber function $Y(x)$, Eqn. (14). Since the Weber function is a type of the Bessel (parabolic cylindrical) functions, this approximation reflects the clustering tendency of global seismicity towards low latitudes, as well as the origin of the North-South preferential orientation of tectonics.

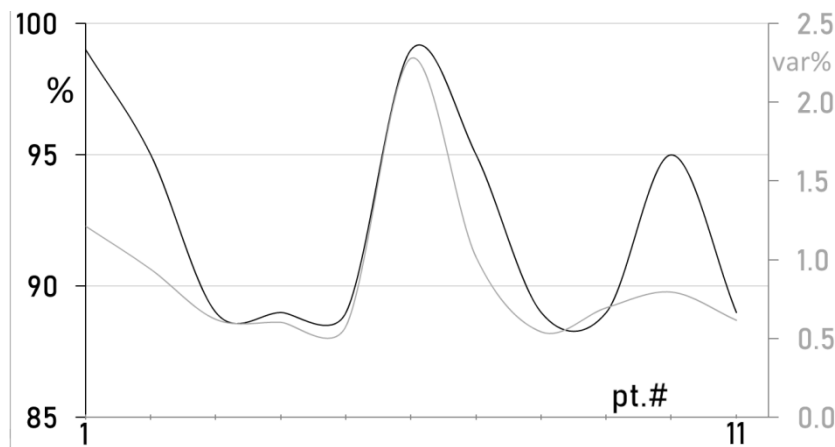


Figure 7. Shown is the change of spectral magnitude in var% (light line) of significant periods clustering at the short end of the 55'-15 days long-periodic Earth band, Table 4, against the change of confidence level (dark line) of the corresponding periods' estimates. Note confidence levels on the estimates never drop below 89% across the entire bundle of 12 peaks (an anomalous peak is not shown; see Discussion), which probably indicates that the cluster is physically meaningful.

Finally, to examine if a random process dominated detection of the sequence of resonance's subperiods (the signal; here the driver phase's fractions), I next compute $s_j^{GVS A}$ of the data with generic seismic magnitudes assigned at random. To make the test rigorous, I specialize the random set to the record's interval of seismic magnitudes $M_w \in (5.5, 8.2)$, thus simulating a comparable real-world situation as closely as possible. Then if strong seismic rupturing is a globally random process (where no global physics influences the extent of structural collapse in solids as measured by emission levels of seismic energies or magnitudes), such a random-data spectrum will also match the theoretical sequence randomly. Otherwise, the so verified non-random process is the driver of the strong seismicity.

Test results, in the form of a matching discrete function Δf , are shown in Figure 8. As can be seen, matches of the $T = 72$ h theoretical resonance subperiods with nearest most significant spectral peaks from real data dominate the first 30 subperiods of the resonance sequence in the 25:5 (83% v. 17%) ratio, thus – since belonging in the strongest-energies part of the band – sufficiently qualifying as the signal driver and hence defining the signal itself. On the other hand, the success of matching beyond the 30th subperiod varies.

However, the 30/42 trade-off seems as such only statistically, but it is not a trade-off in terms of physics since the first 30 subperiods refer to more than 99% of the signal's energy and therefore they are the signal for all physical considerations. Hence the real-data spectra outperform the random-data spectra. As for noise, the seeming trade-off arises since a record rich in geophysical contents including tides as part of the signal (so the record could not be detided), reveals limited information only. Thus the positive detection of the signal's first 30 subperiods, in the absence of any forbidding constraints on the remaining 42 subperiods of signal's noise signature, means a positive detection of the entire sequence of 72 subperiods of the Earth body $T = 72$ h superharmonic resonance.

The weighted average of real-data spectral matching is 2.5% v. random-data matching 8.7% – a 350% outperformance; see Figure 9.

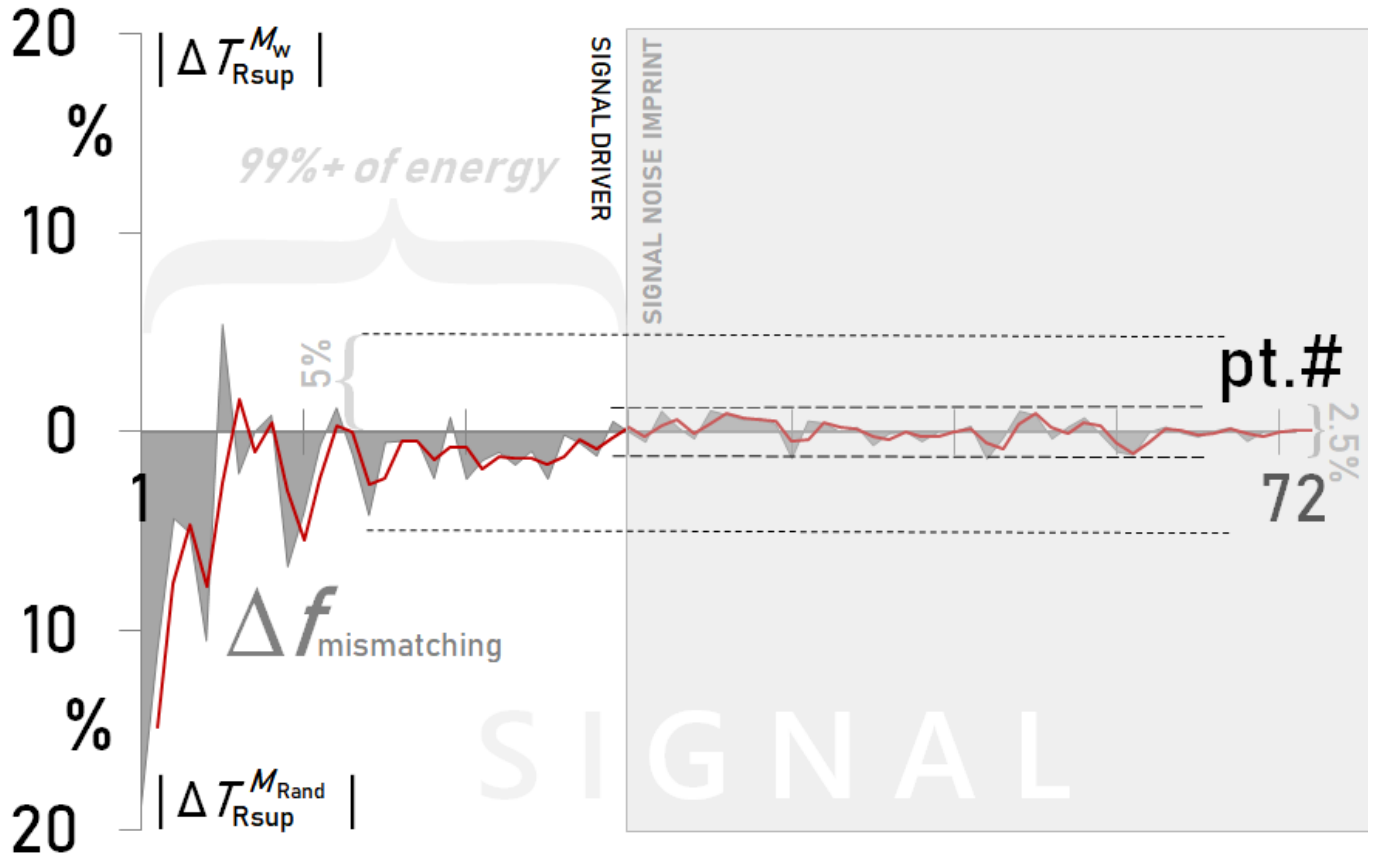


Figure 8. Performance comparison of s_j^{GVSA} from real seismic magnitudes (top half of the plot) v. s_j^{GVSA} from random seismic magnitudes (bottom half of the plot) in representing Earth body resonance faithfully. Zero-value of subperiod means the outperforming of the opposite type of matching along that subperiod. Closer-to-zero-value means a lesser absolute deviation of computed spectra from the theoretical resonance, in percents to the respective resonance subperiod. Detailed description: shown is discrete function $\Delta f_{mismatching}$, as a moving average of absolute differences between each theoretical-resonance subperiod and its respective nearest most significant spectral peaks from real-data seismic magnitudes (top half) v. random-data seismic magnitudes (bottom half), in percentages to the respective theoretical resonance subperiods. Also shown are the declared precision for this research, of $|5\%|$, as well as the matching precision for noise, of 2.5% (the precision of detecting the signal's imprint in noise; however, here any signature is only inferred but unrecoverable for the time being). Data are given in Table 6.

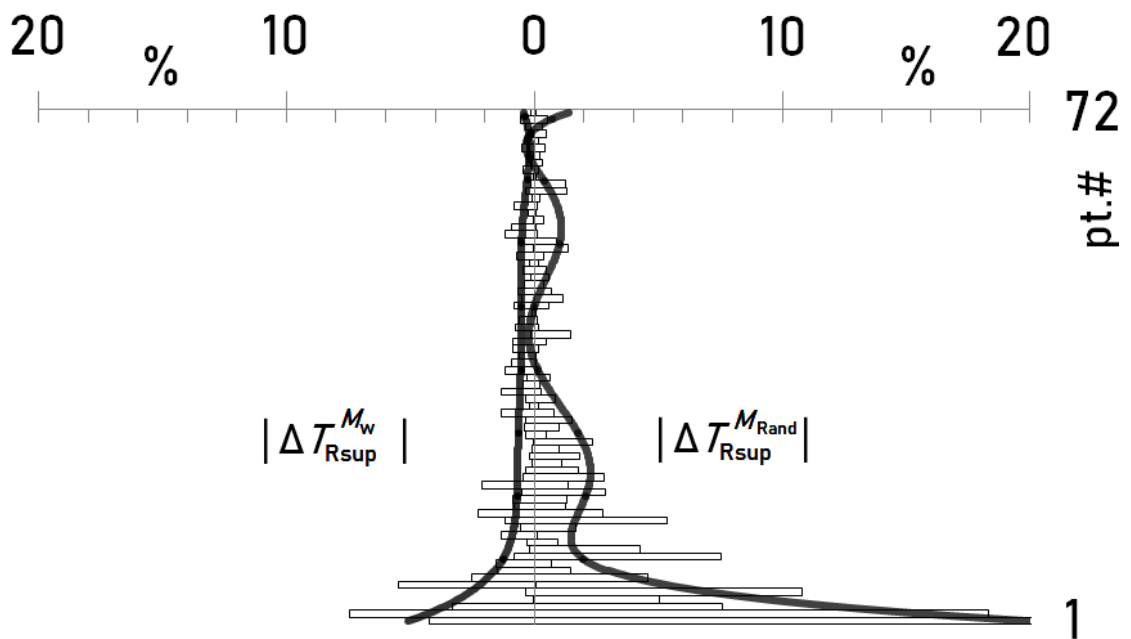


Figure 9. Matches from Table 6 and Figure 8, of real-data (left side) v. random-data (right side) most significant spectral peaks to the nearest theoretical resonance periods, T_{Rsup} , in percents to the theoretical value. With 6th order polynomial trends (black curves).

	T_R' [h]	T_R [h]	T_R^* [h]	ΔT_R [%]	ΔT_R^* [%]		T_R' [h]	T_R [h]	T_R^* [h]	ΔT_R [%]	ΔT_R^* [%]
72/1	72.0000	75.0591	55.4728	4.2488	22.9545	72/37	1.9459	1.9636	1.9470	0.9072	0.0519
72/2	36.0000	33.3241	42.6022	7.4331	18.3394	72/38	1.8947	1.8831	1.8947	0.6142	0.0008
72/3	24.0000	23.2132	25.8251	3.2783	7.6045	72/39	1.8462	1.8305	1.8489	0.8479	0.1505
72/4	18.0000	17.9995	18.9101	0.0028	5.0559	72/40	1.8000	1.8160	1.8089	0.8889	0.4923
72/5	14.4000	14.4466	15.9528	0.3236	10.7834	72/41	1.7561	1.7536	1.7304	0.1422	1.4608
72/6	12.0000	12.6545	11.9933	5.4542	0.0561	72/42	1.7143	1.7016	1.7111	0.7400	0.1862
72/7	10.2857	10.0282	9.8138	2.5036	4.5876	72/43	1.6744	1.6646	1.6767	0.5864	0.1374
72/8	9.0000	8.8661	9.1306	1.4878	1.4515	72/44	1.6364	1.6351	1.6378	0.0772	0.0898
72/9	8.0000	7.8772	7.9454	1.5350	0.6831	72/45	1.6000	1.5869	1.6091	0.8188	0.5704
72/10	7.2000	7.1419	7.7443	0.8069	7.5596	72/46	1.5652	1.5573	1.5468	0.5058	1.1784
72/11	6.5455	6.5321	6.8234	0.2040	4.2461	72/47	1.5319	1.5416	1.5211	0.6322	0.7030
72/12	6.0000	6.0183	6.0580	0.3050	0.9663	72/48	1.5000	1.5062	1.4939	0.4133	0.4055
72/13	5.5385	5.6132	5.5457	1.3494	0.1302	72/49	1.4694	1.4676	1.4606	0.1217	0.5951
72/14	5.1429	5.1709	5.2298	0.5453	1.6900	72/50	1.4400	1.4468	1.4333	0.4722	0.4667
72/15	4.8000	4.7434	5.0569	1.1792	5.3528	72/51	1.4118	1.4091	1.4091	0.1888	0.1900
72/16	4.5000	4.6008	4.6240	2.2400	2.7546	72/52	1.3846	1.3941	1.3899	0.6850	0.3805
72/17	4.2353	4.2008	4.1817	0.8144	1.2660	72/53	1.3585	1.3590	1.3774	0.0375	1.3899
72/18	4.0000	3.9650	4.0525	0.8750	1.3117	72/54	1.3333	1.3412	1.3451	0.5900	0.8813
72/19	3.7895	3.7696	3.8976	0.5244	2.8541	72/55	1.3091	1.2939	1.3105	1.1604	0.1095
72/20	3.6000	3.5236	3.6497	2.1222	1.3811	72/56	1.2857	1.2741	1.2848	0.9033	0.0675
72/21	3.4286	3.4443	3.3318	0.4588	2.8215	72/57	1.2632	1.2636	1.2584	0.0350	0.3743
72/22	3.2727	3.2842	3.2152	0.3506	1.7592	72/58	1.2414	1.2381	1.2414	0.2642	0.0028
72/23	3.1304	3.1275	3.0959	0.0938	1.1034	72/59	1.2203	1.2103	1.2216	0.8226	0.1027
72/24	3.0000	2.9949	3.0547	0.1700	1.8230	72/60	1.2000	1.2008	1.2024	0.0667	0.1994
72/25	2.8800	2.8821	2.9095	0.0729	1.0237	72/61	1.1803	1.1762	1.1961	0.3497	1.3386
72/26	2.7692	2.7691	2.7038	0.0047	2.3615	72/62	1.1613	1.1628	1.1762	0.1300	1.2844
72/27	2.6667	2.6569	2.6802	0.3663	0.5058	72/63	1.1429	1.1425	1.1425	0.0312	0.0278
72/28	2.5714	2.5821	2.5968	0.4150	0.9854	72/64	1.1250	1.1299	1.1230	0.4356	0.1801
72/29	2.4828	2.4911	2.4446	0.3360	1.5351	72/65	1.1077	1.1107	1.1041	0.2715	0.3272
72/30	2.4000	2.4317	2.3812	1.3208	0.7817	72/66	1.0909	1.0909	1.0935	0.0008	0.2418
72/31	2.3226	2.3269	2.3269	0.1860	0.1869	72/67	1.0746	1.0693	1.0794	0.4957	0.4446
72/32	2.2500	2.2580	2.2308	0.3556	0.8532	72/68	1.0588	1.0546	1.0570	0.3989	0.1689
72/33	2.1818	2.1524	2.1883	1.3483	0.2955	72/69	1.0435	1.0438	1.0486	0.0308	0.4893
72/34	2.1176	2.1274	2.1127	0.4606	0.2322	72/70	1.0286	1.0321	1.0321	0.3431	0.3412
72/35	2.0571	2.0514	2.0699	0.2792	0.6183	72/71	1.0141	1.0195	1.0195	0.5340	0.5315
72/36	2.0000	1.9763	1.9978	1.1850	0.1102	72/72	1.0000	0.9984	1.0006	0.1600	0.0586

99% (7, 7)

95% (17, 30)

89% (25, 20)

67% (23, 15)

Table 6. Theoretical, T_R' v. real- and random-data spectral significant periods, T_R and T_R^* , and respective differences, ΔT , in percents to the respective theoretical value.

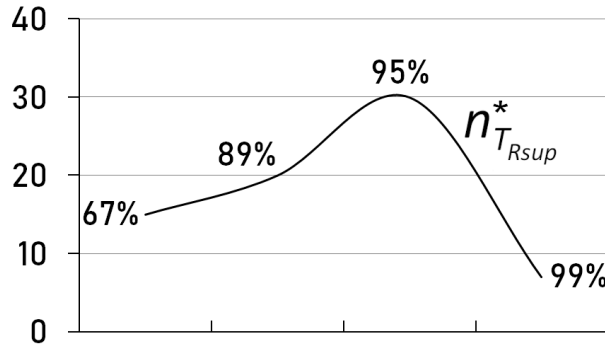


Figure 10. Random-data pseudoquality, as quantified by data responsiveness to estimating significance levels of the detected (range of all) 72 superharmonic resonance periods of the Earth's 3-day phase, from random-data spectra, Table 6 and Figure 8. The plot indicates no genuine response of a physical system to external forcing at long periods, unlike what is seen in Figure 5 from real-data spectra. Shown is the linear response in numbers n_T^* of pseudo-matches to superharmonic resonance periods per confidence level, Table 6.

4. Discussion

The reliable extraction of a complete batch of $p = 72$ superharmonic resonance periods, Table 2, revealed that, in addition to the short-periodic resonant vibration response known as the *Schumann resonances* (extremely long-periodic in the electromagnetic spectrum), the Earth is a mechanical forced oscillator with own fundamental discrete function of the global resonant vibration response in the long-periodic band as well:

$$T_{\text{Rsup}} \in \left[\frac{72}{72}, \frac{72}{71} \dots \frac{72}{2}, \frac{72}{1} \right] \quad (6)$$

or, more generally:

$$T_{\text{Rsup}}(x) : \left| \frac{T}{T + 1 - x} \right| \forall x = 1 \dots p \wedge T \in \mathbb{N} \wedge x \in \mathbb{N} \Big|_1^T, \quad (7)$$

where $T = 72$ h is the resonance-guiding period, x is an independent discrete variable in hours and within its domain of existence $[1 \text{ h}, 72 \text{ h}]$, while $p = 72$ is the resonance range. Note that validity of Eqn. (7) could not be verified for $x > 73$ because, as mentioned in Data Analysis, the 2s-55' band is overburdened with geophysical noise. However, the $x > p$ case is of no concern here, and continuity of Eqn. (7) can be freely assumed on an interval, even an open $x \rightarrow \infty$ (with some caution).

Thus the discrete function extracted from the data as Eqn. (6), and given more generally by Eqn. (7), can be imagined continuous within its domain of existence $[1 \text{ h}, 72 \text{ h}]$, and hence written in an analytical form, as:

$$T_{\text{Rsup}}(x) = \frac{T}{T + 1 - x} \forall x \in \mathbb{R} \Big|_1^T \quad (8)$$

which, for $T = 72$ h, becomes a dimensionless

$$T_{\text{Rsup}}(x) = \frac{72}{73 - x} \forall x \in \mathbb{R} \Big|_1^{72}. \quad (9)$$

The above Eqn. (9) reflects the sum-up, or enveloping, process of the Earth as a seismogenic coupled resonator, and is as such useful for multidimensional modeling of the Earth as a nonlinear oscillatory system. For that purpose, we can also expand the latter into a Taylor series for a real variable $x \in [1h, 72h]$:

$$\begin{aligned}
 T_{\text{Rsup}}(x) &= \frac{72}{73} + \frac{72}{5329} \cdot x + \frac{72}{389017} \cdot x^2 + \dots \\
 &= \frac{72}{73} \cdot \left(1 + \frac{x}{73} + \left(\frac{x}{73} \right)^2 + \dots \right) = \\
 &= \frac{72}{73} \cdot \sum_{u=0}^v \left(\frac{x}{73} \right)^u ; v \in \mathbb{N} \wedge v \gtrsim p,
 \end{aligned} \tag{10}$$

where v is not much greater than the resonance range p but is large enough for Eqn. (10) to converge to the desired precision.

The $T = 72$ h phase dominates the strong earthquakes. This also follows from the detection of its many fractional multiples: $^3/2$, $^{14}/5$, $^5/12$, $^5/36$, etc. This is the first report of any periodicities in tectonic earthquakes occurrences, let alone of a complete range of superharmonic resonance periods including a batch of the Earth's natural mode of oscillation.

The discovery of the overwhelming response of the occurrences of strong earthquakes to the 3-day phase is the evidence of harmonically induced seismotectonics. Besides, the detected superharmonic resonance of the Earth is of $n = T^2$ type, where

$$\frac{n}{m} \gg 1 \Rightarrow n \gg m, \tag{11}$$

characterizes the inducing process.

According to what little is known from mechanical and electrical engineering on subharmonic and superharmonic mechanical resonances in terms of real-life examples, the extracted resonance range, Eqn. (6), is the result of the Earth's phase scaling (acting on) the subharmonic resonance of the Earth as a single externally coupled oscillator:

$$T_{\text{Rsup}} = T \cdot T_{\text{Rsub}}, \tag{12}$$

so that:

$$T_{\text{Rsup}} \in 72 \cdot \left[\frac{1}{2}, \frac{1}{3} \dots \frac{1}{71}, \frac{1}{72} \right]. \tag{13}$$

Alternatively, one could say that the solid Earth acts as both subharmonic and superharmonic mechanical resonator. However, subharmonic and superharmonic resonances are very seldom in Nature or engineering. (Den Hartog, 1985). Besides, the solid Earth's resonance was entirely unknown until now. Furthermore, as already mentioned, only one excitation is required to induce a superharmonic resonance (Yang & al., 2016), and the excitation of the Earth's resonance by the Moon has been demonstrated as the absolutely largest and driving the Earth forcer phase (Omerbashich, 2007). Then the Earth resonance as reported herein makes, to the best of author's knowledge, a new class of superharmonic resonance, Eqn. (11). Then this paper warrants a closer look into general superharmonic properties of the Earth as a strictly nonlinear system.

As seen in Figure 6, the difference between theoretical v. computed spectra that have revealed the Earth's superharmonic resonance, Figure 3, is most likely due to data resolution, Figure 5. Specifically, although the longest three periods in Table 2 seem like outliers, the longest estimate's fidelity was $\Phi_{\text{Rsup}} \gg 12$, whereas a $\Phi > 12$ indicates a physically meaningful result (Omerbashich, 2006b). Note also the gradual deterioration rather than an uneven change in the three longest periods' divergence from respective theoretical values. At first sight, the difference seems best modeled by a (mother) half-wavelet function. But because of a fixed precision of the spectral analysis and finiteness of the resonance range (discreteness of the resonating masses), the difference could, in reality, reflect the overall system's response in the form of a fast-converging Bessel function of 2nd kind called the Weber function:

$$Y_e(x) = \lim_{l \rightarrow e} \frac{J_l(x) \cos l\pi - J_{-l}(x)}{\sin l\pi}; \quad l \in \mathbb{N} \wedge e \in \mathbb{N}, \quad (14)$$

where

$$J_l(x) = \sum_{z=0}^{\infty} \frac{(-1)^z \left(\frac{x}{2}\right)^{l+2z}}{z! \Gamma(l+z+1)}. \quad (15)$$

This outcome is largely due to the linear representation of background noise-levels in GVSA spectra, and would not be so readily discernible from power spectra, i.e., Fourier class of spectral methods. Since the Weber function is a type of the Bessel (parabolic cylindrical) functions, this approximation reflects the known tendency of global seismicity to cluster in location towards low latitudes, as well as the origin of the known North-South preferential orientation of Earth tectonics. That, in turn, points at a unique nature of the $M_w 6.2+$ strong seismicity as a global process, while realistically reflecting the fact that that seismicity tends to arise on a parabolic cylinder enveloping the Earth in the equator, as the strong earthquakes cluster towards the equator while avoiding frigid zones. Since this conclusion was reached solely by studying a global $M_w 6.2+$ seismicity time-series, global seismicity and tectonics are one and inseparable process in the realm of the georesonator hypothesis as well as in reality.

Importantly, the Earth's natural or characteristic mode of oscillation, T_E , is also strongly present in the computed spectra of earthquake occurrences: as a 55-64' cluster at the 99–67% confidence levels, see Figure 4 and Table 4. Assuming signal split in the shortest part of the band, due to the Earth largely – though never entirely – damping its vibration because of its internal viscosity (Den Hartog, 1985), it is physically justifiable to average that spread. This gives the mean of 1.0025 h, see Table 4. Remarkably, the absolutely strongest resonance period detected was 0.9984 h at 2.3 var%, which was at the same time centered on the Earth natural mode's cluster; see Figure 2 and Table 2. The mean between the measured normal period and its cluster-averaged value is 01^h 00' 01.62" or 1 h exactly to within twice the 1Hz sampling rate. This remarkable precision, due largely to the GVSA (Omerbashich, 2007), strongly suggests that the here discovered superharmonic resonance is the modulator of the Earth's natural mode via *synchronization*, which is usually defined as the ability of coupled oscillators to lock to a common period (Pikovsky & al., 2001) (Thévenin & al., 2011). Then the most probable value of the Earth's natural mode is 1 h. Resonance-assisted synchronization of coupled oscillators via frequency locking but not necessarily phase locking has been demonstrated for nonlinear physical systems (Thévenin & al., 2011) – such as the Earth under conjunctions at which an additional nonlinearity is introduced via gravitational vector's disturbing ("stirring") of Earth masses aperiodically though repeatedly.

The Earth is a nonlinear oscillating system damped due to viscosity – but incompletely so due to external forcing. It makes sense then to examine if such a system is also self-excited – in addition to being both freely and forcedly excited – and thereby nonlinear in a most complex way possible (Den Hartog, 1985). Here, such a demonstration follows directly from the computed spectra which reveal an anomalous (inside the Earth normal mode's cluster) yet virtually 99%-significant period of 55.67' at a high 1.1 var%, Figure 2. The anomalous period is well defined though slightly shorter than the damped Earth's natural period discerned as 1.00 h. Since damping lengthens the self-excited system's natural period somewhat with respect to the period of self-excited vibration (Den Hartog, 1985), the 55.67', Figure 2, seems to be the period of self-excited vibration. If true, this proposed period confirms the key role of Earth's self-vibration as well as free and forced oscillations.

Remarkably, the anomalous period is globally (laterally and depth-wise as the data did not discriminate in the sense of depth stratification) so stable/key that the said 2% data-removal affected neither the period itself nor its variance-based spectral magnitude estimates. While it can be shown that seismic strong motion generally belongs in locally stationary random processes (Elghadamsi & al., 1988), stability of the anomalous peak's variance-based magnitude with quasi-temporal change indicates a quasi-random and therefore quasi-deterministic (having asymptotic probabilities) stationary process as well, for the entire time-series – meaning both spatially- and temporally-globally. So due also to the spatio-temporal nature of the analyzed time-series, the earthquakes responsible for the anomalous period did not arise on a fault due to the fault's causal determinism and thermal-chemical conditions, but mechanically-regionally instead – as part of the regional structural collapse due to a self-vibrating resonance of plates and regions. (Here, a self-induced resonance of the total-mass Earth is excluded from considerations for obvious reasons.) Add the intrinsic nonlinearity of the external forcing, and one is led to conclude that the Earth is, in fact, an oscillating system (a system critically composed of many independently and dependently oscillating bodies of mass – oscillators), which is at the same time overwhelmed with a most complex nonlinearity. Such a high level of complexity makes testing of the analyzed time-series for stationarity very difficult, or at least until the complexity has been successfully decomposed so that the self-vibrating resonance peaks are separated, extracted, and analyzed. The signal's stability, along with its demonstrated clarity cf. staying above a confidence level over the entire resonance range, and strength as seen by the band's highest peak being strongest in the natural period's own bundle as well – demonstrated beyond doubt that virtually all of $M_w 6.2+$ seismicity arises due to long-periodic resonance.

In order to describe Earth's multi-oscillatory dynamics, simple classical second-order differential equations stemming from the Newtonian mechanics, such as

$$\ddot{X}(\tau) = F(X(\tau)); F(X(\tau)) \perp \dot{X}, \quad (16)$$

while sufficing for many types of nonlinear problems in geophysics, astrophysics, and astronomy, will not be adequate here. Advantages of algebraic, namely tensorial, representations of the multidimensionality aspect of the Earth's multi-oscillatory dynamics, ought to be used as well.

Based on the preceding discussion, Table 2 and Figure 2 show that the Earth is a many-oscillator system in which the number of oscillators is somewhat less or equal the number of tectonic plates and mantle's semi-rigid regions combined. Presently, at least 159 tectonic major, minor, and microplates have been identified or proposed, while their dynamics has been a subject of speculation (Harrison, 2016). The number and dynamics of brittle regions in the upper mantle are unknown. With whatever structural information on each oscillator at our disposal, approximations such as the Kuramoto method and its many variations, which describe the behavior of a large number of coupled oscillators on a circle (Kuramoto, 1975), could be applied for different latitudes. To complicate things even more though, the 100s of Earth's own oscillators are most likely only weakly coupled, so that their own normal modes

poorly synchronize with each other as well as with the Earth's 3-day phase. Other complications include time-dependent vibration disorder and delayed coupling due to the moving of the plates and mantle, and so on. However, much can be gained from data in order to recover the governing equations of the Earth as a sparsely identified nonlinear dynamical system (Brunton & al., 2016).

Since this is the first report ever of any periodicities bundle in earthquakes occurrences, let alone of a complete range of superharmonic periods including the Earth's natural oscillation period, seismotectonics on our planet arises via resonant response of different lithosphere chunks and mantle's brittle regions. Each of those mass subsystems features its own natural period at which such a body of mass experiences a resonant rupture (an earthquake) when their natural period matches a here detected superharmonic resonance period or its fractional subperiod, becoming the resonant period. Foreshocks or aftershocks are experienced during synchronization or quieting of a resonating body of mass relative to an Earth's resonant frequency, respectively. Note that what is reported in here represents detection of only one external forcer; however, that is sufficient to induce resonance in a nonlinear system such as the Earth under irregularly repetitive conjunctions acting as the forcing disturbance.

Because the data were prepared so to fit a previously postulated hypothesis, the here reported result represents a solid proof of that hypothesis's validity, and an evidence of the extraterrestrial cause of seismotectonics via frequency demultiplication as one of the rarest mechanical phenomena in Nature, known for its ability to magnify the energy injected at the fundamental disturbing frequency by 100s of times (Den Hartog, 1985).

While this study has succeeded in extracting some of the information most valuable for earthquake prediction to date, it should be noted that any modeling of subharmonic and especially superharmonic resonance is difficult. Nevertheless, direct earthquake prediction in terms of timing, strength, and location of the rupturing should follow from this discovery in a more-less straightforward manner. In the meantime, numerical approximations and stochastic approaches such as seismic forecasting remain of enormous value.

This report brings an immediate and important advancement in predictive abilities of seismology, as the primary task of any science: it enables highly reliable anti-forecasting for M6.2+ seismicity, months ahead and anywhere on Earth. Thus, while a positive forecast states a chance of an earthquake, a negative or anti-forecast states a chance of no earthquake (Harris, 1998). Then in light of the herein unveiled physical mechanism of global resonance seismotectonics, anti-forecasting can also be understood as a direct prediction of seismic quiescence. For it has been too often asserted that a successful seismic prediction is only the one that can predict earthquake's location, time, and size (magnitude); see, for example (Wyss & Dmowska, 1997). Trying to satisfy this all-or-none approach has turned out futile, and insisting on the absolute direct prediction has been impractical. Such, a most stringent, requirement, is found in no other science. The anti-forecasting as proposed here is accomplished directly by identifying the times without conjunctional external forcing.

Note that, although the mathematical generalization of the here reported discovery's background hypothesis has also revealed a relationship between the Earth's normal mode of oscillation and the Moon's orbital period at both macroscopic and quantum scales, this discovery is not about matching of orbital periods (gravitational or orbital resonance). It is about the magnification of mechanically resonating masses oscillation that arises due to conjunctions indirectly. Specifically, the primary gravitational effect or the pull (push, in some modern approaches in physics) is insufficient as the seismicity modulator. Instead, during conjunction, the resonance balance (between viscously induced damping and celestially induced excitation) – observed as a permanent seismic hum in the geophysical band (Nishida, 2014) and maintained thanks to all possible gravitational vectors acting on the Earth interior simultaneously – gets disturbed. Specifically, the only way for the Earth to behave like such an undamped oscillator is if the energy gets supplied to the system externally. At the same time, no momentum or force has been added in the classical sense, so all additions only mean more hum (mum, in fact). Conjunctions merely take away from that mum. Thus, a secondary gravitational effect is at work, which arises

due to the gravitational vectors' stirring of the Earth masses as its body rotates. And that is the main external contributor to the nonlinearity of the Earth as a physical system. Mechanical magnifying oscillators were explored by many in the past, notably Maxwell and Tesla.

When discussing complex mechanical oscillators it is impossible to avoid the subjects of electricity and magnetism. It has been long speculated in geophysics that co-seismic phenomena observed in the electromagnetic domain as seismic precursors mean that seismicity is fundamentally an electromagnetic phenomenon. However, that electromagnetic precursors to $\sim M6+$ strong seismicity do not mean an electromagnetic seismogenesis – but are instead a byproduct of key seismogenic mechanical interactions – is seen from the fact that, while neither Mars nor Venus possesses bodily magnetic fields (Stevenson, 2010), Mars, unlike Venus, however does not partake in forming of strong seismicity on Earth as described by the pattern, Figure 1 (Omerbashich, 2016). In addition, while electromagnetic phenomena indeed precede some strong earthquakes, in most earthquakes that does not happen. Thus electromagnetic seismic precursors suggest an occasional reaction of the medium to the seismicity-generating mechanism instead. Electromagnetism in seismology is a useful but non-essential phenomenon.

As demonstrated in this paper: while electromagnetic precursors occur at random, the **strong seismicity is a global quasi-deterministic physical process caused by the dynamics of the rotating Earth as an externally forced nonlinear mechanical oscillator whose moving parts act like weakly coupled oscillators themselves, and whose own natural frequencies occasionally match one of the Earth's superharmonic resonance frequencies or its fraction, resulting in an $M6.2+$ earthquake.** Seismicity is not caused by electromagnetism but by the progenitor mechanical vibrations, as magnetic fields and electromagnetic forces arise naturally in a magnifying mass-oscillator at work such as the Earth (Den Hartog, 1985) (Omerbashich, 2007).

5. Conclusions

I have demonstrated that the Earth's seismotectonics arises in a harmonic response of tectonic plates and upper-mantle regions to the Earth's domicile range of 72 resonance periods, shown completely recoverable from USGS, EMSC, and GFZ catalogs of $\overline{M_w}5.6+$ occurrences. The discovery is real since the signal represents a dominant carrier resonance (on which the seismicity "rides" as it occurs), rather than a physical process that was inserted seismically into some intermediary data. The detection of an entire resonance range in the band commonly referred to as "long-periodic noise" (but which was here shown abundantly rich in useful information) means that the resonance is unceasing and that all tectonic plates and regions respond actively to some of the resonance periods as those activate. Both internal and external factors induce the Earth's body resonance. The Earth acts as a multi-mechanical oscillator under a constantly albeit unevenly supplied and externally induced forcing that, along with self-vibration, makes our planet a quasi-deterministic nonlinear system with a 3-day phase and ~ 10 m maximum displacement.

When analyzed with spectral techniques impervious to uneven spacing of a time-series, the catalogs are also shown rich with spectral clusters such as a fully recoverable signal of the Earth's natural period of 1 h arising due to the Earth's synchronization to the celestial forcing and for other reasons. The discovery has two important consequences. Immediately, it enables reliable $M_w6.2+$ anti-forecasting (seismic quiescence prediction). In the long run, it points earthquake research in a new direction – of studying subharmonic and especially superharmonic properties of the Earth as a forced, many-oscillator system with dynamically changing nonlinearity. The identification of the system's governing equations from the earthquake and other data should result in successful conceptualizations of Earth-tailored physically-based earthquake prediction.

This discovery nullifies the heat-transfer hypothesis, which should radically diminish the significance of geochemistry and other applications of chemistry in geosciences.

References

- Brunton, S., & al.** (2016). Discovering governing equations from data by sparse identification of nonlinear dynamical systems. *Proceedings of the National Academy of Sciences (PNAS)* 113(15):3932-3937.
- Den Hartog, J.** (1985). *Mechanical Vibrations* (4th ed.). New York: Dover Publications.
- Dziewonski, A., & al.** (1981). Determination of earthquake source parameters from waveform data for studies of global and regional seismicity. *Journal of Geophysical Research - Solid Earth* 86(B4):2825-2852.
- Elghadamsi, F., & al.** (1988). Time-dependent power spectral density of earthquake ground motion. *Soil Dynamics and Earthquake Engineering* 7(1):15-21.
- Harris, R.** (1998). *The Loma Prieta, California, Earthquake of October 17, 1989 - Forecasts*. Washington DC: U.S. Geological Survey.
- Harrison, C.** (2016). The present-day number of tectonic plates. *Earth, Planets and Space* 68:37-51.
- Kanamori, H.** (1977). The energy release in great earthquakes. *Journal of Geophysical Research - Solid Earth and Planets* 82(29):2981-2987.
- Kuramoto, Y.** (1975). Self-entrainment of a population of coupled non-linear oscillators. (H. Araki, Ed.) *Lecture Notes in Physics* 39:420-422.
- Nishida, K.** (2014). Source spectra of seismic hum. *Geophysical Journal International* 199:416–429.
- Omerbashich, M.** (2016, August 31). Astrophysical cause of tectonics. (C. Yuntai, Ed.) *Earthquake Science*. In press.
- Omerbashich, M.** (2004). *Earth-model discrimination method*. Ann Arbor, Michigan, USA: ProQuest.
- Omerbashich, M.** (2006b). Gauss-Vaníček Spectral Analysis of the Sepkoski Compendium: No New Life Cycles. *Computing in Science and Engineering* 8:26-30.
- Omerbashich, M.** (2007). Magnification of mantle resonance as a cause of tectonics. *Geodinamica Acta* 20:(6):369-383.
- Omerbashich, M.** (2019). On solar origin of alleged mass-extinction periods in records of natural data. (A. Y. Rozanov, Ed.) *Paleontological Journal*. In press.
- Omerbashich, M.** (2006a, August 20). Springtide-induced magnification of Earth mantle's resonance causes tectonics and conceals universality of physics at all scales. arXiv. New York, USA. <http://de.arxiv.org/abs/physics/0608026>
- Pikovsky, A., & al.** (2001). *Synchronization: A Universal Concept in Nonlinear Sciences* (Vol. 12). Cambridge, United Kingdom: Cambridge University Press.
- Press, W., & al.** (2007). *Numerical Recipes: The Art of Scientific Computing* (3rd ed.). London, United Kingdom: Cambridge University Press.
- Schröder, W., & Treder, H.-J.** (1997). Einstein and geophysics: Valuable contributions warrant a second look. *EOS Trans. AGU* 43(78):479–485.
- Stevenson, D.** (2010). Planetary Magnetic Fields: Achievements and Prospects. *Space Science Reviews* 152:651–664.
- Tesla, N.** (1919). The magnifying transmitter. *Electrical Experimenter* VII(74):112-113,148,173,176-178.
- Thévenin, J., & al.** (2011). Resonance Assisted Synchronization of Coupled Oscillators: Frequency Locking without Phase Locking. *Physical Review Letters* 107:104101(1-5).
- Vaníček, P.** (1969). Approximate Spectral Analysis by Least-Squares Fit. *Astrophysics and Space Science* 4(4):387–391.
- Vaníček, P.** (1971). Further Development and Properties of the Spectral Analysis by Least-Squares Fit. *Astrophysics and Space Science* 12(1):10–33.
- Wyss, M., & Dmowska, R.** (1997). Earthquake prediction – state of the art. *Pure and Applied Geophysics (PAGEOPH)* 149(1):350.
- Yang, J., & al.** (2016). Vibrational subharmonic and superharmonic resonances. *Communications in Nonlinear Science and Numerical Simulation* 30(1-3):362–372.